TRITA-MEK
Technical Report 1999:08
ISSN 0348-467X
ISRN KTH/MEK/TR--99/08--SE

Development of guide-vanes for expanding corners with application in wind-tunnel design

Björn Lindgren

June 1999
Technical reports from
Royal Institute of Technology
Department of Mechanics
SE-100 44 Stockholm, Sweden

1 Introduction

In the mid 1990s it was decided that the wind-tunnel resources at the Department of Mechanics, Royal Institute of Technology, had to be complemented by another low speed wind-tunnel with similar characteristics, but smaller than the large MTL low speed wind-tunnel currently used at the department. The similar characteristics means that projects and experiments first can be tested in the new wind-tunnel, making it possible to use the time in the large wind-tunnel more effectively. The new wind-tunnel can also replace the old small wind-tunnel at the department for some of the student experiments in various fluid mechanics courses and thereby get the students in contact with modern wind-tunnel technique already in the undergraduate education. In the beginning an open type wind-tunnel was planned but the idea was later rejected because of inconveniences, such as noise and air turbulence in the room.

In 1995, during a major renovation of the building, space was made available for the new tunnel in the basement of the laboratory where the MTL wind-tunnel is located. By use of a sub-basement area for the return part a standing wind-tunnel circuit was achieved. This layout has the benefit of occupying the least space possible and the noise and vibrations from the fan is kept away from the test section. Only one major problem was now left to be solved before the construction could start. The wind-tunnel circuit was too short for the size of test section planned and a contraction ratio of 9. The contraction ratio is the ratio between the largest and the smallest cross section in the wind-tunnel. It was decided to investigate the possibilities of using expanding corners to solve this problem.

Expanding corners are corners with a larger outlet area than inlet area. The idea of expanding corners is to use the guide-vanes to help with the expansion in the wind-tunnel circuit. The large expansion ratio, in our case 1.32 in each corner, makes it possible to save as much as 30 % in wind-tunnel circuit length with a given test section size and contraction ratio. This means that a larger test section and a higher contraction ratio is possible for a given building location.

The idea of using expanding corners is not new although this is the first wind-tunnel that has incorporated the feature. There were experiments as early as in the 1930s and the idea has been tested a few times since then. Some experiments are done by [Collar, 1936], [Friedman and Westphal, 1952], [Kröber, 1932] and [Wolf, 1957]. The conclusions from these experiments was though always that the traditional approach with non-expanding corners and conventional diffusers was better. The problem with these experiments is that they used guide-vanes with very poor design and for expanding corners to work the guide-vanes have to be optimized for each particular expansion ratio. Otherwise it is likely that the guide-vanes are not able to sustain the high loads and high pressure gradients present in an expanding corner.

To see if it was possible to use expanding corners with the expansion ratio we wanted an experimental setup was built. This was a small open wind-tunnel with one corner. The expansion ratio of this corner could be changed between 1 and $\frac{5}{3}$. The cross section area in front of the corner was 0.3 m by 0.3 m and the maximum speed was 25 m/s. It was also possible to adjust the vane angle of attack and the distance between the vanes. One important parameter is the spacing to chord ratio which is the distance between the vanes normalized with the chord length.

The guide-vanes used were a scaled-down version of the vanes used in the MTL tunnel. These vanes are designed so that the flow on the suction side will not separate even if the boundary layers are laminar. The two-dimensional total pressure loss coefficient, defined as the loss of total pressure normalized with the dynamic pressure, is as low as 0.036 at a Reynolds number of 154000. This is in fact an extremely low loss compared to ordinary vanes which typically have losses that are four times as large.

The results from these experiments were very encouraging. It was shown that very large expansion ratios were possible. Even at the highest expansion ratio tested, $e = \frac{5}{3}$, the two-dimensional total pressure loss coefficient was as low as 0.15 at a Reynolds number of 200000 and a spacing to chord ratio of 0.27. With the expansion ratio, $e = 1.32$, and with the spacing to chord ratio, $\epsilon = 0.27$, we had chosen for the wind-tunnel corners the total pressure loss coefficient was 0.055 using the MTL scaled-down guide-vane at a Reynolds number of 200000.

To study the performance of the guide-vanes the profile was analyzed by the use of the MISES program, a two-dimensional cascade flow solver with a built-in module for optimizing vane-shapes. This program solves a coupled Euler-boundary layer equation system. It can handle moderate separation and separation bubbles, but at massive separations the iteration procedure does not converge.

Calculations showed similar results as the experiments for moderate expansion ratios but at larger values of this ratio it under-estimated the total pressure loss coefficient indicating that the flow remained attached at much higher expansion ratios than in the experiments.

The pressure distribution on the surface of the tested guide-vane showed that it was possible to improve the shape, eliminating laminar separation bubbles on each side of the vane. At the reattachment points for these bubbles the boundary layers are turbulent and they were located very close to the leading edge. The guide-vane used in the experiments was used as a start profile in the calculations. The optimization module in MISES is inverse in the meaning that the pressure distribution is specified and the program then alters the shape of the vane profile trying to achieve a pressure distribution equal to the stipulated one. The changes in the pressure profile has to be moderate though for the process to converge. The result from this optimization was a guide-vane with a different camber and thickness distribution as well as a slightly larger nose radius to avoid separation at moderate deviations of the angle of attack. The new guide-vane has a calculated total pressure loss coefficient of 0.041 which is slightly higher than for the MTL guide-vane in a non expanding corner but still very much better than most vanes designed for use in wind-tunnels today.

When an acceptable guide-vane had been developed it was time to start the design of the new wind-tunnel incorporating expanding corners. To test different design ideas a program was developed that calculates pressure and velocity profiles along the wind-tunnel circuit as well as the pressure losses. It also calculates the power necessary to drive the fan and the cooling power needed to keep a steady temperature in the test section whatever velocity chosen. The dimension of the test section and the overall maximum and minimum dimensions were set. There were also possibilities to change the location of different parts as coolers and fan and it was also possible to change the number of screens and the contraction ratio. The parts were then matched so that they would fit together. After deciding upon the size and location of the fan and the cooler the detailed construction began.

The 12 blade axial fan is driven by a 15 kW AC motor controlled by a frequency converter. Two silencers, one on each side of the fan achieve a low noise level in the test section and act as converters between square and circular cross sections. Some expansion is also taking place in the silencers all in order to achieve a very compact tunnel circuit.

A heat exchanger is installed after the third corner and it is able to maintain a constant temperature over the whole speed range. It provides for a fast and steady temperature control in the test section. The temperature variation in time is $\pm 0.03°$ C and the variation over the cross section area is $\pm 0.07°$ C.

Each corner has an expansion ratio of 1.316. The reason for choosing this expansion ratio is that with a contraction ratio of 9 and the expansion in the vertical plane in the corners and the expansion in the horizontal plane in the diffusers the expansion ratio becomes $\sqrt[8]{9} \approx 1.32$. Measurements behind the first corner downstream of the test section confirmed the expected good performance of the guide-vanes in the expanding corner and showed that the total pressure-loss coefficient is as low as 0.046. The value obtained in the calculations was 0.041 for a somewhat lower Reynolds number. Three-dimensional effects should be expected to increase the total pressure loss for the measurements.

The diffusers used in this wind-tunnel are two-dimensional. Normally three-dimensional diffusers are used but here the expanding corners take care of the expansion in the vertical plane, which is the key to the compact circuit design. Two-dimensional diffusers are not as effective in pressure recovery as three-dimensional diffusers. They are also more prone to separation, but the actual diffusers used have been shown to be free of separation. One special feature in this wind-tunnel is that the first diffuser downstream of the test section has variable diffuser angle making it possible to use the test section more efficiently.

Screens and honeycomb are important parts in obtaining a good flow quality. They have here been chosen to be of a design similar to that used in the MTL wind-tunnel.

The most important part for the flow quality is without doubt the contraction. The mean flow relative variations are reduced by a factor CR^2 in the streamwise direction and $\sqrt{CR}$ in the cross-stream direction. With the present contraction ratio of 9 the reduction in the streamwise direction is thus 81 times. The shape of the contraction must be carefully designed to avoid separation. The present contraction shape was chosen to be the same as in the MTL tunnel and have been shown to be free of boundary layer separation.

The part where the experiments in a wind-tunnel takes place is the test section. It is here 4 m long and the cross section area is 0.5×0.75 m^2. The top and bottom walls of the test section is filled with hatches for good accessibility. One side wall is also removable allowing large equipment, such as boundary layer plates, to be easily installed. This wall can also be replaced to suit specific needs of different types of experiments. The idea here is to allow users to prepare and test some of their experimental equipment without the need for direct access to the tunnel. The removable wall is also adjustable along the flow direction allowing the pressure gradient to be set. Often it is desirable to have zero pressure gradient and with growing boundary layers on the test section walls and measurement equipment. This means that the cross section area has to grow along the downstream direction.

To study the flow quality in the test section and thereby evaluating the entire wind-tunnel design measurements were performed over the cross section 0.25 m from the beginning of the test section. The measurements were performed at a flow speed of about 25 m/s. Comparisons with the large low speed wind-tunnel, MTL, is taken from [Johansson, 1992].

The total pressure variation normalized with the dynamic pressure in the test section varies ± 0.1 %. In terms of velocity variation, it is equal to ± 0.05 %. These variations are similar to those in MTL indicating that the contraction is functioning well and emphasizes the importance of the contraction ratio which is the same in both wind-tunnels.

Flow deviation variations in the cross section is within $\pm 0.1°$. This is also in the same order of magnitude as for MTL. The five screens and the honeycomb removes possible flow angle deviations in the last corner in the intended way.

The power factor for the wind-tunnel circuit was estimated to be 0.46 at a flow speed of 46 m/s. This value is well in line with the calculated value in the preliminary study. The corresponding value for MTL is 0.39 at a flow speed of 69 m/s. One must bear in mind that the power factor is strongly dependent on the Reynolds number with a decreasing value for increasing Reynolds number.

The conclusions from these measurements is that the wind-tunnel project has been successful. Further calibration measurements still have to be performed, including single-wire and cross-wire hot-wire anemometry. The concept of expanding corners has attracted some interest both nationally and internationally. For instance, the new wind-tunnel at Mälardalen University includes expanding corners with the guide-vane design developed here.

2 Summary of papers

There are two papers included in this licenciate thesis. The first paper consists of measurements and calculations on guide-vanes in expanding corners. It also includes optimization of a guide-vane for the expansion ratio 1.32. The results from these investigations was later used in the design of the new wind-tunnel. Paper 2 treats the design procedure of the wind-tunnel and it also contains results from the calibration work that has been done to fine tune the wind-tunnel for optimum performance.

3 Acknowledgments

The author would like to thank his supervisor Professor Arne Johansson for the opportunity to be a part of such a major project as the design and construction of a new wind-tunnel. I am also grateful for the support and ideas from Jens Österlund, Ulf Landén and Marcus Gällstedt. Finally I gratefully acknowledge the funding from the Göran Gustafsson Foundation and TFR.

References

[Collar, 1936] Collar, A. R. (1936). Some experiments with cascades of aerofoils. A.R.C. Technical Report 1768, Aeronautical research committee.

[Friedman and Westphal, 1952] Friedman, D. and Westphal, W. R. (1952). Experimental investigation of a 90° cascade diffusing bend with an area ratio of 1.45:1 and with several inlet boundary layers. TN 2668, NACA.

[Johansson, 1992] Johansson, A. V. (1992). A low speed wind-tunnel with extreme flow quality-design and tests. *Proc. the 18:th ICAS Congress*, pages 1603–1611.

[Kröber, 1932] Kröber, G. (1932). Schaufelgitter zur Umlenkung von Flussigkeits-Strömung. *Ingenieur-Archiv*, 3:516.

[Wolf, 1957] Wolf, H. (1957). Messungen im Nachlauf eines Gleichdruckgitters für 90°-umlenkung. *Maschinenbautechnik*, 6(10):539.

Experiments in Fluids 24 (1998) 265–272 © Springer-Verlag 1998

Measurement and calculation of guide vane performance in expanding bends for wind-tunnels

B. Lindgren, J. Österlund, A. V. Johansson

Abstract The design of guide vanes for use in expanding bends was investigated both experimentally and numerically. The primary application in mind is the use of expanding corners in wind-tunnels for the purpose of constructing compact circuits with low losses. To investigate the performance of guide vanes in realistic situations expansion ratios between 1 and $\frac{5}{3}$ were tested in the experiments. These were carried out in an open wind-tunnel specially built for the present purpose. The experimental results demonstrated that suitably designed guide vanes give very low losses and retained flow quality even for quite substantial expansion ratios. For wind-tunnel applications expansion ratios around 1.3 seem appropriate, Optimization of a guide vane design was done using a two-dimensional cascade code, Mises. A new vane optimized for an expansion ratio of $\frac{4}{3}$ gave a two-dimensional total pressure-loss coefficient as low as 0.041 for a chord Reynolds number of 200,000.

1 Introduction

In closed wind-tunnels the requirement of attached flow in the diffusers is often a major factor in determining the total length of the circuit. In the present work we investigate the idea of using expanding corners equipped with guide vanes to reduce the need for diffusers in wind-tunnel applications. Actually, the use of expanding corners could also be of interest in various other applications, such as ventilation systems.

Expanding corners with low losses would both reduce the total losses and give the possibility of increasing the length of the test section for a given circuit length. Space restrictions are often serious limiting factors when wind-tunnels are designed. Expanding corners offer a promising way to obtain a compact circuit if a good performance of the guide vanes can be guaranteed.

Many wind-tunnels use $\frac{1}{4}$-circle-shaped vanes with prolongation at the trailing edge. Such vanes have a three-dimensional total pressure-loss coefficient of typically 0.20, see Klein et al. (1930). This is about 4 times as much as for an optimized profile. It is not, however, always the lowest pressure-loss coefficient that is desirable. Also good flow quality is essential, especially in the corner upstream of the setting chamber.

The present work includes both an experimental and a numerical investigation of guide vane performance in expanding 90° bends. The experiments cover a range of Reynolds numbers, vane spacings and area ratios. The numerical calculations were done both for comparison with the experimental results and to optimize a new vane for expanding corners.

The experiments were performed in a small test tunnel built specifically for this purpose. It is an open tunnel, with a 300×300 mm^2 straight section upstream of the corner connected to the downstream variable area section. The tests covered a chord Reynolds number range up to 230 000. The total pressure-loss coefficient was determined and the behaviour of the flow was studied with the aid of smoke visualization.

During the construction of the MTL wind-tunnel at KTH a guide vane was developed and optimized for a non diffusing corner at low Reynolds numbers. A first part of this study is reported by Sahlin and Johansson (1991), pertaining to vanes designed to have turbulent boundary layers. The ones finally used in the MTL-tunnel at KTH were designed to have laminar boundary layers. An already good understanding of its behaviour and the very low pressure-loss achieved in a corner using this vane made it suitable for the new application. The two-dimensional pressure loss coefficient is below 0.04 for this vane at a chord Reynolds number of 200,000.

These vanes were tested in expanding corners and found to give quite satisfactory results. A new vane was also designed and optimized for the situation in an expanding corner.

The present results will be used in the construction of a new wind-tunnel at KTH, where the corner expansions are used to accommodate a total area expansion of a factor of three. Plane diffusers, with the expansion only in the direction normal to the plane of the tunnel circuit, are then used to give a further area increase by a factor of three. Hence, a total contraction ratio of nine is achieved with a quite moderate need of diffusers, yet with an expansion ratio of about 1.32 in each

Received: 7 April 1997/*Accepted*: 11 August 1997

B. Lindgren, J. Österlund, A. V. Johansson
Royal Institute of Technology
Department of Mechanics
SE-100 44 Stockholm, Sweden

Correspondence to: A. V. Johansson

The authors are grateful to Professor Mark Drela at MIT for supplying the MISES code. We wish to thank Mr. Alexander Sahlin and Mr. Per Åke Thorlund for valuable comments on the design of guide vanes. We are grateful to Mr. Ulf Landén and Mr. Marcus Gällstedt who helped with the manufacturing of the experimental apparatus. We also wish to thank NUTEK for the financial support.

corner. The results presented in this work show that this can be achieved with very small losses in the corners, and a good quality of the flow exiting the corners.

2
Methods of calculating total pressure-loss coefficient and lift coefficient

When the flow passes through a sharp bend equipped with guide vanes, the pressure field is set up by the ensemble of vanes and the walls. Hence, instead of analyzing a single vane, one has to analyze a cascade of vanes.

2.1
The total pressure-loss coefficient

The quantities needed to be measured in the experiments are the difference between total and static pressure at position 1 and the difference between atmospheric pressure and static pressure at position 0 and 1, respectively. Position 0 is located upstream of the corner and position 1 is located downstream of the corner (see Fig. 1).

The total pressure-loss coefficient is defined as

$$\frac{\Delta H}{q_0}=\frac{p_{t0}-\overline{p_{t1}}}{q_0} \tag{1}$$

where p_{t0} is the total pressure at position 0 and $\overline{p_{t1}}$ is the mean value of the total pressure over the cross-section at position 1. ΔH is the average total pressure-loss in the corner and q_0 is the dynamic pressure at position 0. The dynamic pressure at position 0 is defined as

$$q_0=\tfrac{1}{2}\rho U_0^2 \tag{2}$$

where U_0 is the flow velocity at position 0. The mean value of the total pressure at position 1 is

$$\overline{p_{t1}}=\frac{1}{nh_1}\int_0^{nh_1} p_{t1}(y)\,\mathrm{d}y \tag{3}$$

where n is the number of vanes over which the integration is performed and h_1 is the spacing between the vanes perpendicular to the outflow direction, see Fig. 2.

If the frictional resistance in the inlet is neglected Bernoulli's theorem gives that q_0 is the difference between the atmospheric pressure and the static pressure at position 0. Hence,

$$q_0=p_{atm}-p_0 \tag{4}$$

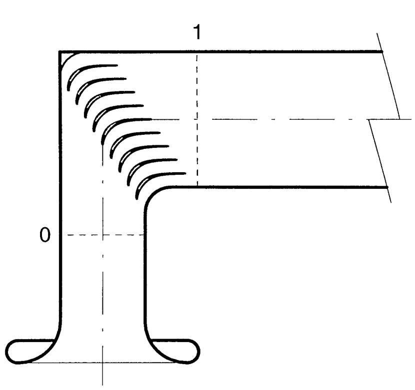

Fig. 1. The guide-vane corner with the measurement positions 0 and 1

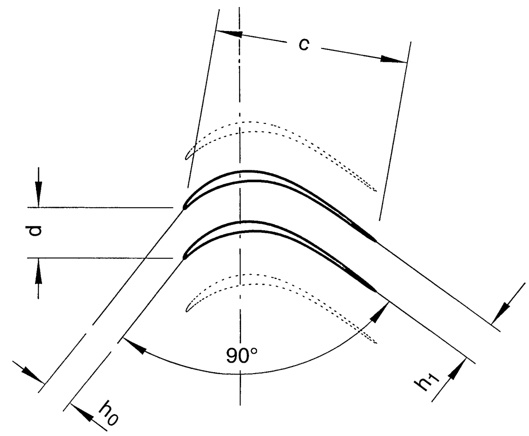

Fig. 2. The cascade geometry

The same reasoning yields that the total pressure at position 0, p_{t0}, is equal to the atmospheric pressure,

$$p_{t0}=p_{atm} \tag{5}$$

Combining Eqs. (1), (3), (4) and (5) results in the following expression for the total pressure-loss coefficient written on a form displaying the pressure differences measured in the experiments,

$$\frac{\Delta H}{q_0}=\frac{p_{atm}-p_1-\frac{1}{nh_1}\int_0^{nh_1}(p_{t1}(y)-p_1)\,y}{p_{atm}-p_0} \tag{6}$$

2.2
Calculation of lift coefficient

From the momentum theorem, the following expression for the lift-force on a 90° expanding bend, can be derived.

$$L'=2q_0\frac{d}{e} \tag{7}$$

where L' is the lift force per unit length in the spanwise direction and d is the spacing between the vanes, see Fig. 2. The expansion ratio, e, is defined as

$$e=\frac{h_1}{h_0} \tag{8}$$

where h_0 and h_1 is the spacing between the vanes perpendicular to the inflow and outflow directions respectively, see Fig. 2.

The total pressure-loss over the cascade, ΔH, is

$$\Delta H=\frac{D'}{d} \tag{9}$$

where D' is the drag per unit length in the spanwise direction.

This results in the following expression for the total pressure-loss coefficient,

$$\frac{\Delta H}{q_0}=\frac{2}{e}\frac{D'}{L'} \tag{10}$$

Note that the lift-to-drag ratio in equation (10) refers to the entire corner and not just a single vane. In other words it is important not only to maximize the lift-to-drag ratio for a single vane but also to reduce the number of vanes needed in the cascade.

The dimensionless lift coefficient is defined as

$$c_{L'} = \frac{L'}{1/2\,\rho c u^2} \tag{11}$$

where c is the vane chord and u is the flow speed over the vanes. The question is now which flow speed is the most representative for this case. The most important factor affecting the flow characteristics is obviously separation, which normally will start at the trailing edge of the vane (Fig. 2). Therefore the flow speed at the trailing edge is chosen for normalization in expression (11). It now reads

$$c_{L'} = \frac{L'}{1/2\,\rho c (U_o/e)^2}. \tag{12}$$

Introducing the dimensionless pitch, ε, defined as the vane spacing to chord ratio,

$$\varepsilon = \frac{d}{c} \tag{13}$$

results, together with Eqs. (2), (7) and (12), in the following equation for the lift coefficient

$$c_{L'} = 2\varepsilon e. \tag{14}$$

3 Experimental apparatus

The wind tunnel, see Fig. 3, used in the experiments was constructed especially for this purpose, although the fan with upstream and downstream silencers existed as parts of an older test rig.

3.1 The wind-tunnel used in the experiments

The tunnel is of the open-suction-type with an inlet equipped with a contraction (1), (numbers referring to Fig. 3), with an area ratio of 9.

The straight section upstream of the corner, (2), has an area of 300×300 mm^2 and a length of about 400 mm to ensure uniform inflow conditions for the corner vanes. In this section the static wall pressure is measured at a location 300 mm downstream of the inlet, at half tunnel height. Extra care has been taken to achieve good quality pressure taps. This is very important when measuring static pressure (Shaw, 1960).

The 90° corner, (3) has a constant inlet area, and is adaptable to the expansion ratios, 1, $\frac{4}{3}$, $\frac{3}{2}$, $\frac{5}{3}$ by varying the outlet width to 300, 400, 450 and 500 mm, respectively, keeping the tunnel height constant at 300 mm. The corner walls are given a radius of curvature of 77.5 mm.

The guide vanes (91L198) tested are of the same design, although somewhat smaller than those used in the MTL low turbulence wind-tunnel at KTH. They are optimized for a non-expanding corner with a pressure-loss coefficient for such a situation that has been shown to be very small. They are made of aluminium extruded at SAPA, Sweden. Their span is 282 mm and the chord is 196 mm. This gives an aspect ratio of about 1.44 (Fig. 4).

To minimize the secondary flow over the vanes at this low aspect ratio, the wall boundary layers have to be controlled. This is achieved by separating the vanes 8 mm from the wall boundary layers. Small $\frac{1}{4}$-circle plates guide the boundary layer flow through the corner.

A mechanism enabled the angle of attack of the guide vanes to be easily adjustable in order to obtain the desired outflow angle which is achieved by measuring the static wall pressure 300 mm downstream from the corner.

The straight section downstream of the corner, (4), is made with an adaptive wall that enables the desired expansion ratio to be set. A pair of static wall pressure sensors is located 110 mm downstream from the inner radius at half tunnel height.

Sect. (5–9) include a diffuser, a transformation from a square to a circular cross section, silencers, a fan and another diffuser to increase the top speed of the wind-tunnel.

The speed range is from 0 to 25 m/s upstream of the corner giving a maximum chord Reynolds number of 325,000.

3.2 Measurement equipment

The measurements were made with a total pressure tube, 2 mm in diameter and 100 mm long. It was attached to a 400 mm long tube, 8 mm in diameter, which could be traversed in the cross-stream direction with a resolution of about 10 μm.

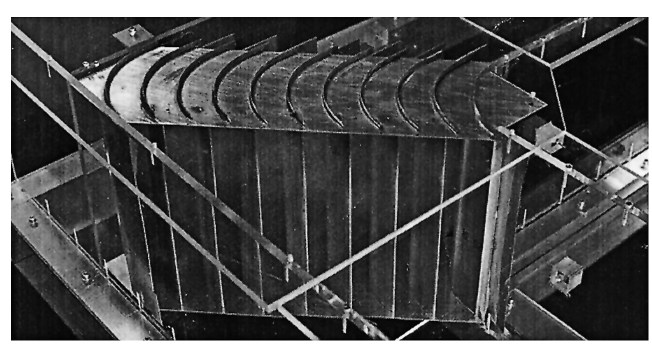

Fig. 4. The guide vanes at expansion ratio 1

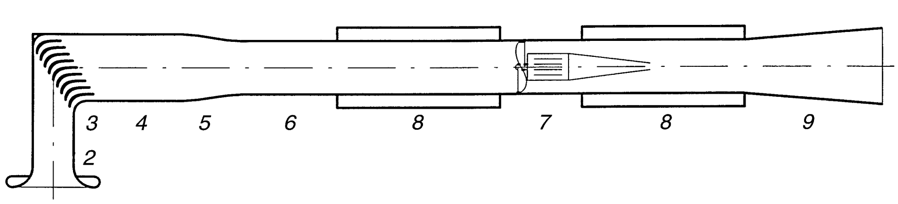

Fig. 3. The wind-tunnel used in the experiments. Expansion ratio $e = \frac{5}{3}$

A high accuracy (Furness Controll FC012) micromanometer was used for the pressure measurements.

4
Measurements of the total pressure-loss coefficient

Four series of measurements were carried out to investigate the dependence of the two-dimensional total pressure-loss coefficient on the key flow parameters. First, measurements with a pitch (spacing to chord ratio) of 0.27 were made at the expansion ratios 1, $\frac{4}{3}$, $\frac{3}{2}$ and $\frac{5}{3}$. Then, two different expansions, $\frac{4}{3}$ and $\frac{3}{2}$, were used to investigate the effects of the Reynolds numbers in the range from 25,000 to 230,000. In a third series measurements the influence of the pitch was examined with the pitch ranging from 0.27 to 0.39. The aim was to find an optimum pitch for the expansion ratio $\frac{4}{3}$. The final type of comparative measurements studied the three expansion ratios, 1, $\frac{4}{3}$ and $\frac{3}{2}$, with the vanes having the same lift coefficient. The Reynolds number was 200,000 in all measurements except the Reynolds number variation experiment.

4.1
Variation of expansion ratio for constant pitch

The total pressure-loss coefficient increases with increasing expansion. There is reason to assume that the rate of increase becomes higher at large expansion ratios because of boundary layer separation on the vanes. In order to investigate this behaviour, expansion ratios as large as $\frac{5}{3}$ were tested.

A Reynolds number of 200,000 was selected because it is high enough to make the pressure loss fairly independent of small variations, but still low enough to represent typical flow speeds of low-speed wind-tunnels. In this case, with a vane chord of 196 mm, the velocity is about 15 m/s.

The pitch chosen is the same as in the MTL low turbulence wind-tunnel at KTH which is motivated by the fact that the vanes used in the experiments are of the same type as in that tunnel. The MTL-tunnel does not have expanding corners though. This pitch (0.27) is not an optimized value for the total pressure-loss coefficient, but is instead optimized for low disturbances in the flow and the vanes are thus able to take higher loads, occurring on expanding corners.

The results for different expansion ratios indicate indeed that there is a possibility to successfully incorporate the expanding corner element into the design of wind-tunnels (see Fig. 5). The results were very encouraging even at rather large expansion ratios. A more dramatic increase of the two-dimensional total pressure-loss coefficient was found only between the two highest expansion ratios.

The pressure distribution at position 1 is shown in Fig. 6 for an expansion ratio of $\frac{4}{3}$. For this expansion ratio flow over the vanes is essentially attached and the loss is only marginally higher than for the non-expanding case. The wake profiles for the largest expansion, on the other hand, indicate substantial separation of the vane boundary layers.

4.2
Variation of Reynolds number

The Reynolds number dependence of the total pressure-loss coefficient was studied at the two expansion ratios, $\frac{4}{3}$ and $\frac{3}{2}$. For non-diffusing corners with attached laminar flow on the vanes

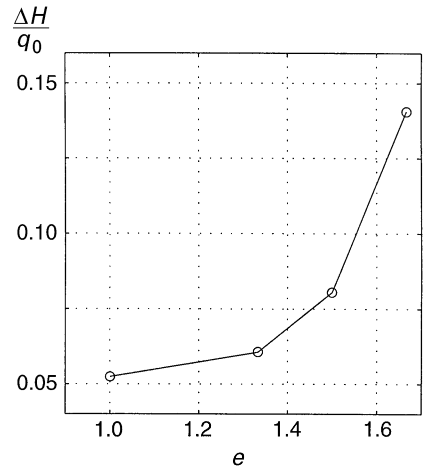

Fig. 5. The total pressure-loss coefficient as a function of the expansion ratio. $Re = 200{,}000$ and $\varepsilon = 0.27$

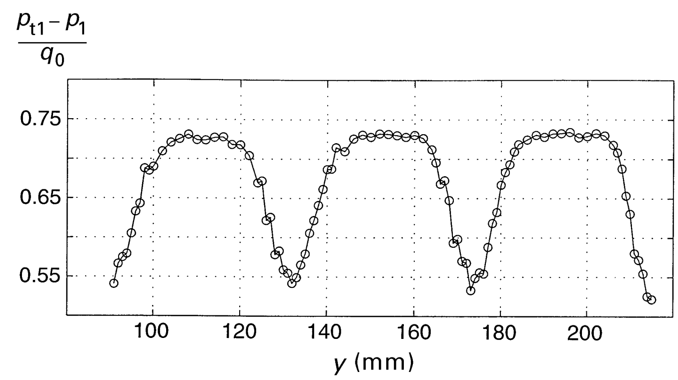

Fig. 6. Typical wake pressure distribution. $e = \frac{4}{3}$, $\varepsilon = 0.27$ and $Re = 200{,}000$

the normalized loss varies approximately as

$$\frac{\Delta H}{q_0} \sim \frac{1}{\sqrt{Re}} \qquad (15)$$

The two measurement series with varying Reynolds numbers for expansion ratios of $\frac{4}{3}$ and $\frac{3}{2}$ gave similar results, although somewhat less favourable for the larger expansion, see Fig. 7. Hence, as might be expected, low-Reynolds number effects seem to be more severe at larger expansions.

At the lower Reynolds number studied, about 25,000, the flow speed is only 1 to 2 m/s which makes the measurements rather inaccurate and sensitive to disturbances caused by air movements in the laboratory outside the inlet of the open tunnel.

For the smaller expansion, $\frac{4}{3}$, we can observe a behaviour in Fig. 7 that is approximate in agreement with that expected from a completely laminar attached flow. Hence the slope is close to $-\frac{1}{2}$ in the log-log plot (cf Eq. (15)). At the higher expansion ratio the slope is smaller at low Reynolds numbers. Thereafter the total pressure-loss coefficient first begins to decrease faster than at lower Reynolds numbers, but with increasing Reynolds number the decrease in the value of the coefficient slows down again. An explanation for this behaviour could be that the flow is separated at low Reynolds

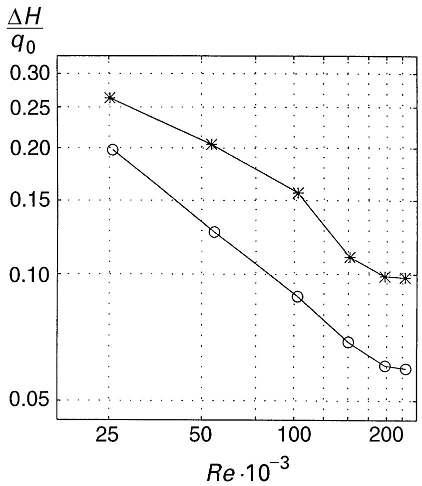

Fig. 7. The total pressure-loss coefficient as a function of the Reynolds number. ⋆: $e = \frac{3}{2}$ and $\varepsilon = 0.24$, ○: $e = \frac{4}{3}$ and $\varepsilon = 0.27$

numbers, and at some higher value there is a reattachment creating a separation bubble. Downstream of the reattachment the flow is most probably turbulent, and the relative increase seen at high Reynolds numbers may then be interpreted as being caused by turbulent skin friction over an increasing part of the vane as the separation bubble becomes smaller. This behaviour would qualitatively explain the appearance of the curve for $\frac{3}{2}$ in Fig. 7, however this phenomenon has to be examined further.

4.3
Variation of pitch

The pressure-loss variation with pitch was investigated with the aim of finding an optimum at an expansion ratio in the range that would be of interest for wind-tunnel applications. This was chosen here as $\frac{4}{3}$. The optimum should be expected to vary somewhat with the expansion ratio. Actually a minimum of the total pressure-loss may not be the optimum solution in a more general sense since stability and flow quality also must be considered.

To find the vane spacing with the lowest value of the total pressure-loss coefficient, a series with the pitch ranging from 0.24 to 0.39 was performed. The results in Fig. 8 exhibit a minimum at a rather high value of the pitch, about 0.35. At this high value, the flow is most probably separated, but because of the thickness of the profiles and the frictional resistance they produce, a certain amount of separation leads to lower losses since fewer vanes are needed. The Reynolds number used here was 200,000. At lower Reynolds numbers separation tends to occur more easily, and the optimum value for the pitch will then be somewhat lower. The behaviour of the total pressure-loss coefficient as a function of the pitch indicates a sharp increase for pitch-values higher than the optimum value.

4.4
Variation of expansion ratio for constant lift coefficient

To best illustrate how the total pressure-loss coefficient varies with varying expansion ratio, one should perhaps make the comparison for equal loading of the vanes. By choosing $\varepsilon = 0.27$ for the expansion ratio $\frac{4}{3}$, we get a lift coefficient from Eq. (14) of 0.72, which should not be too high for this type of vane. With equal lift coefficient for the expansion ratios 1, $\frac{4}{3}$ and $\frac{3}{2}$ we obtain pitch values of 0.24, 0.27 and 0.36 for each expansion ratio, respectively.

Hence, in this measurement series the expansion ratio is varied under conditions such that the lift coefficient is held constant. This gives perhaps the most direct indication on how well every particular expansion functions. The increase in the total pressure-loss coefficient was found to be slightly stronger than in the case with the same pitch for every expansion, see Fig. 9. The Reynolds number was the same in both series, about 200,000, which enables a direct comparison between the results in Figs. 5 and 9.

4.5
Summary of the experimental results

It is clear from the above that the idea of expanding wind-tunnel corners works well if the expansion is not too large and the Reynolds number is kept reasonably high. A good

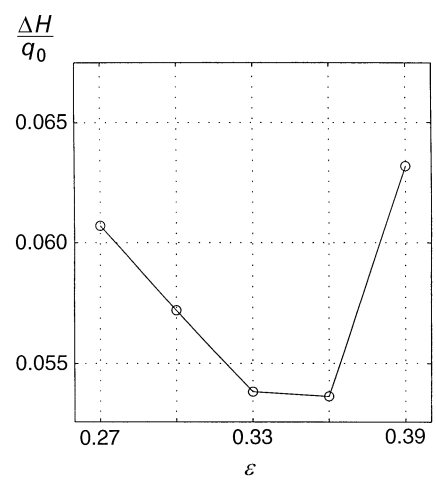

Fig. 8. The total pressure-loss coefficient as a function of the pitch. $e = \frac{4}{3}$ and $Re = 200{,}000$

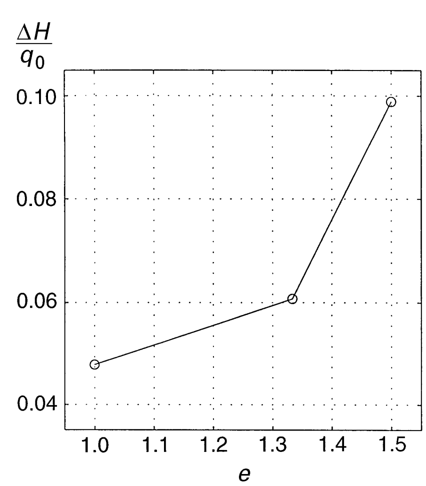

Fig. 9. The total pressure-loss coefficient as a function of the expansion ratio. $Re = 200{,}000$ and $c_{L'} = 0.72$

performance requires fairly well designed vanes but even vanes optimized for non-expanding corners can work well if designed to accommodate the lift coefficients occurring in the expanding corner.

With vanes optimized for a particular expansion the results will obviously be better. In the present investigation the vanes used were originally designed for non-expanding corners. A configuration with these vanes for an expansion ratio of $\frac{4}{3}$ and a pitch between 0.33 and 0.36 gives a total pressure-loss coefficient of less than 0.054 at a Reynolds numbers of about 200,000. A vane optimized for a non-diffusing corner was found by Sahlin and Johansson (1991) to give a two-dimensional total pressure-loss coefficient of about 0.036 at $Re = 154{,}000$. The increase in total pressure-loss is 50% for the expanding case.

If we choose to compare cases with equal lift coefficient, the $\frac{4}{3}$ expansion has a two-dimensional total pressure-loss coefficient of 0.061 to be compared with 0.048 for the non-expanding case, i.e. a 27% loss increase caused by the expansion.

We may also have in mind that typical vanes today in wind-tunnels are designed as $\frac{1}{4}$-circle-shaped vanes with prolongation at the trailing edge. For a non-expanding corner such vanes give a three-dimensional total pressure-loss coefficient of about 0.20, see (Klein et al. 1930).

5
Calculations of infinite cascade with experimental vane and vane optimization

Numerical calculations matching the Reynolds numbers and the expansion ratios with those in the experiments, give an opportunity to further study the values of the losses and pressure distributions around the vanes. They also provide information on the level of acuracy of the measurements.

Since the tested vane is optimized for non-expanding flows there are cases where parts of the flow are separated when the vane is used in an expanding corner. Abrupt increases of the pressure coefficient, C_p, in the pressure distribution of the vane will indicate where the separation takes place. A profile more optimized for an expansion ratio of $\frac{4}{3}$ is also developed.

5.1
The numerical code used in the calculations

The numerical calculations are made with the MISES code. MISES is a collection of programs for cascade analysis and design, including programs for grid generation and initialization, flow analysis, plotting and interpretation of results, and an interactive program to specify design conditions. MISES was developed by Harold Youngren and Mark Drela to analyze turbo-machinery design.

Mises first generates an incompressible 2-D panel solution to find the stagnation streamlines. It also locates iso-potentials at the vane edges. The streamlines and iso-potentials are used to generate the grid.

On the grid generated previously Mises solves steady Euler equations coupled with integral boundary layer equations using a Newton-Raphson method. This makes it possible to analyze flows with strong viscous/inviscid interactions like shock induced separation flows or separation bubbles. However, this requires the flow to be compressible. The minimum Mach number needed is in the range of 0.10–0.15. This is small enough not to significantly affect the results for incompressible cases.

Optimizations of vane shapes can be performed with the help of an inverse method. Two different inverse methods are available, one suited for large modifications and one suited for detail modifications. In these methods the pressure distribution of the vane can be altered at wish and a number of modified Chebyshev polynomials are used to change the shape of the vane to fit the specified pressure distribution. These polynomials can be modified according to the users requests. The changes in the pressure distribution, however, has to be moderate to achieve convergence. This means that the optimization process has to be repeated a considerable number of times before major improvements are reached. It is also possible to edit the blade shape in the blade editor. However, only basic editing modes like rotate, translate and scale are available.

For further information on the Mises code see Youngren and Drela (1991), Drela and Youngren (1995), Giles and Drela (1987).

5.2
Calculations of infinite cascades with the experimental vane

The losses calculated in the MISES code are matching the losses obtained in the experiments quite well at moderate expansion ratios (see Fig. 10). However at higher expansion ratios the agreement is not very good. The losses from the computations show only a sight increase with increasing expansion ratio. Hence, the computations do not capture the large effects of separation at large expansion ratios. Three-dimensional effects will also disturb the two-dimensional measurements resulting in a faster increase of the losses than in the numerically calculated solutions which are purely two-dimensional.

The pressure distribution around the vane at the expansion ratio $\frac{4}{3}$ clearly indicates that it was not designed for expanding corners (see Fig. 11). On the lower surface there is a small separation bubble near the leading edge, and on the upper surface there is another but larger separation bubble about $\frac{1}{3}$

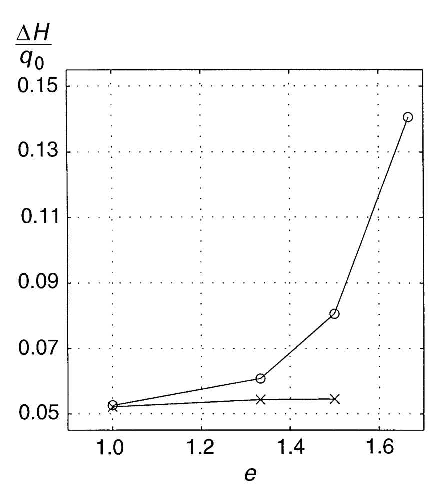

Fig. 10. The total pressure-loss coefficient as a function of the expansion ratio. $\varepsilon = 0.27$ and $Re = 200{,}000$. ×: computations, ○: experiments

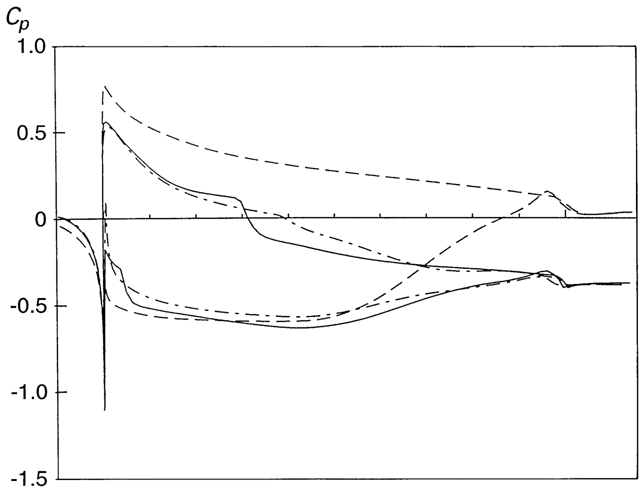

Fig. 11. Pressure distribution for 91L198 at $Re = 200{,}000$. Solid line: $e = \frac{4}{3}$ and $\varepsilon = 0.27$. Dashed line: $e = 1$ and $\varepsilon = 0.3$ (design point). Dash-dotted line: new vane (L27132B) with $e = \frac{4}{3}$ and $\varepsilon = 0.27$

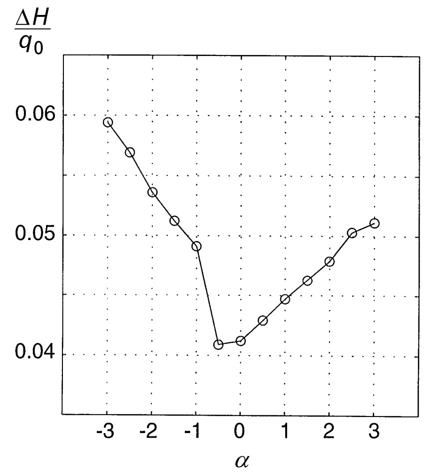

Fig. 12. The total pressure-loss coefficient as a function of the angle of attack, α. $e = \frac{4}{3}$, $\varepsilon = 0.27$ and $Re = 200{,}000$

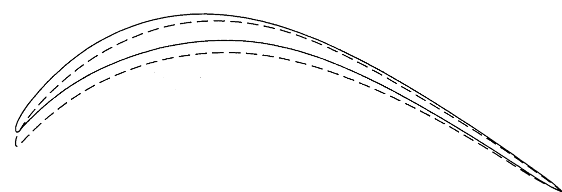

Fig. 13. Solid line: 91L198 optimized for non-expanding corners, $e = 1$ and $\varepsilon = 0.3$. Dashed line: L27132B the new vane optimized for expanding corners, $e = \frac{4}{3}$ and $\varepsilon = 0.27$

downstream of the leading edge. These features have a negative effect on the performance of the vane, and the losses can be reduced substantially in an optimization process.

The vane is also quite sensitive to variations in the angle of attack. Especially the first corner in a wind-tunnel is exposed to significant variations in the angle of attack where the disturbances from the test section are of considerable strength.

Numerical calculations with variations in the Reynolds number indicate an increase in the size of the separation bubbles with decreasing Reynolds number. The separation bubble on the upper surface also tends to move downstream with decreasing Reynolds number. For sufficiently small Reynolds number (or high loads), the flow will separate entirely from the vane. The MISES code is not able to reproduce this behaviour since it only accepts small wakes.

As long as the expansion ratio is moderate, the numerical calculations and the experimental results agree well. This means that the numerical calculation method can be used in the optimization process which could lead to a new profile design that better suits the particular conditions of expanding corners.

5.3 Optimization of a vane for the $\frac{4}{3}$ expansion ratio

When a new vane, emerging from the inverse process, fulfills the requirements of the designer one has to bear in mind that the profile is only optimized for the given Reynolds number, pitch, angle of attack and expansion ratio. To create a vane, that can be used under other circumstances than those specified in the optimization process, it is normally not meaningful to push the optimization too far for any given set of parameters. It is more important to assure that the vane can operate within a wide spectrum of flow conditions. This may lead to slightly larger losses but it will not have a major influence on, e.g., the overall losses of the wind tunnel.

The main goal of this optimization was to minimize and, if possible, eliminate all separation bubbles. The separation bubbles generate both transition from laminar to turbulent boundary layers and rapid increase in the pressure. With the new vane the influence of separation bubbles has been substantially reduced. (Fig. 11).

To improve the tolerance to variations in angle of attack the leading edge radius was enlarged. This resulted in a slightly larger total pressure-loss but increased the ability to perform with up to 3 degrees of negative angle of attack (Fig. 12).

The new vane is designed for a Reynolds number of 200,000, but it has been tested numerically for Reynolds numbers between 100,000 and 600,000. The total pressure-loss coefficient decreases rapidly with Reynolds number between 100,000 and 200,000, but for Reynolds numbers higher than 200,000 the decrease in total pressure-loss coefficient is small.

The conditions under which the optimization was performed is essential when comparing the results with other calculations or experiments. The Reynolds number, pitch and expansion ratio all have a strong impact on the final results, both in terms of losses and optimum vane shape. This new vane has a total presure-loss coefficient of 0.041 with a Reynolds number of 200,000, a pitch of 0.27 and an expansion ratio of $\frac{4}{3}$.

The differences in profiles of the experimentally tested vane and the new design, L27132B, suited for expanding corners are illustrated in Fig. 13. Coordinates representing the shape of the new vane can be found in Lindgren et al. (1997).

6 Discussion

Among early studies of guide vanes for corners in wind-tunnels we may mention (Collar, 1936; Klein et al. 1930; Kröber, 1932;

Wolf, 1957). An investigation of expanding corners that also include control of the boundary layers was carried out by Friedman and Westphal (1952). They studied a 90° cascade expanding bend with an area ratio of 1.45 : 1 and with several inlet boundary layers. Despite the rather simple design of the vanes used in that study quite promising results were obtained with a three-dimensional, but with thin boundary layers, total pressure-loss coefficient as low as 0.11. The total pressure-loss coefficient was almost independent of the Reynolds number that was varied between 330,000 and 950,000.

The present results show that a more sophisticated vane design can reduce this significantly and that it is indeed possible to construct expanding corners with small additional losses as compared to non-expanding ones.

This has several implications for the design of wind-tunnel circuits, but could also be used in a number of other applications, such as ventilation systems. For wind-tunnels it opens possibilities to substantially reduce the length of the return circuit without increasing the risk for separation in the diffusers. Actually, there are often conflicting requirements in connection with the construction of wind-tunnels to fit in the circuit within a given space and to have as large a test section as possible.

A possibility is also to reduce the total losses in the circuit by reducing wall friction losses and by enabling a larger cross sectional area at the second corner, thereby reducing the losses there. In traditional circuit design the diffuser between the first and second corner is quite short so that the second corner will have a cross sectional area not much larger than the first, and thereby comparable losses.

For large expansion ratios large regions of the flow will be separated, and the mean flow will be non-uniformly distributed with higher velocities near the inner radius. In the present study this phenomenon was visualized by smoke, which however was only possible at low Reynolds number (and may perhaps not be wholly representative for high Reynolds numbers). Also, three-dimensional secondary flow effects increase with increasing expansion. These drawbacks were quite negligible though at moderate expansion ratios, such as 1.33.

The geometry in an expanding corner is also somewhat different from an ordinary corner. In contrast to non-expanding corners the imaginary line from the centre of the inner radius to the centre outer radius does not go through the points where the straight walls meet. This means that the whole package of vanes is translated downstream in the tunnel. The relative position between the vanes also differs from the non-expanding case. This implies that there is room for significant improvements in the vane geometry from that optimized for the non-expanding situation. This was also clearly demonstrated by the new vane L27132B. Perhaps even better results can be achieved if the vane is designed to have a turbulent boundary layer on the upper surface. With the fast increase in pressure along the chord which is a result of the expansion in the corner it is very difficult to maintain a laminar boundary layer on the upper surface. A vane designed to have turbulent boundary layers may therefore in some respects be a better starting-point in the optimization process.

The lift force on the vanes changes direction with changing expansion. This called for adjustments in the profile geometry. The absolute value of the lift force decreases with increasing expansion. This improves the efficiency of the expanding corner solution.

A suitable methodology that one may adopt in wind-tunnel circuit design with expanding corners is the following. Let us first define the x–y plane as the plane defined by the circuit centreline. For a given contraction ratio, C_R, and a contraction section with equal distortions in the two lateral directions, we can then choose to take the total x–y plane expansion, $\sqrt{C_R}$, in the corners, and the z-expansion in the diffusers. The diffusers will hence be plane with this approach, and will have a total area increase of a factor $\sqrt{C_R}$, only. The expansion in each corner becomes $C_R^{1/8}$ if the epansion is chosen to be the same in all corners. For instance, with a contraction ratio of 9, the expansion in each corner becomes approximately 1.32. This value will vary only slightly over the range of interesting contraction ratios because of the small value of the exponent ($\frac{1}{8}$).

Many alternative approaches are, of course, possible, depending on the design requirements in the specific case.

References

Collar AR (1936) Some experiments with cascades of aerofoils. A.R.C. Technical Report 1768. Aeronautical Research Committee

Drela M Youngren H (1995) A users guide to MISES 2.1. MIT Computational Aerospace Sciences Laboratory

Friedman D; Westphal WR (1952) Experimental investigation of a 90° cascade diffusing bend with an area ratio of 1.45 : 1 and with several inlet boundary layers. TN 2668, NACA

Giles MB; Drela M (1987) Two-dimensional transonic aerodynamic design method. AIAA J 25: 1199–1206

Klein GJ; Tupper KF; Green JJ (1930) The design of corners in fluid channels. Canadian J of Research 3: 272–285

Kröber G (1932) Schaufelgitter zur Umlenkung von Flüssigkeits-strömungen. Ingenieur-Archiv 3: 516–541

Lindgren B; Österlund J; Johansson AV (1997) Measurement and calculation of guide vane performance in expanding bends for wind tunnels. TRITA-MEK 1997:6, Department of Mechanics, KTH

Sahlin A; Johansson AV (1991) Design of guide vanes for minimizing the pressure loss in sharp bends. Phys Fluids A 3: 1934–1946

Shaw R (1960) The influence of hole dimensions on static pressure measurements. J Fluid Mech 7: 550–564

Wolf H (1957) Messungen im Nachlauf eines Gleichdruckgitters für 90°-Umlenkung. Maschinenbautechnik 6: 539–545

Youngren H; Drela M (1991) Viscous/inviscid method for preliminary design of transonic cascades. In: AIAA, SAE, ASME, and ASEE, Joint Propulsion, Conference, 27th

DESIGN AND CALIBRATION OF A LOW SPEED WIND-TUNNEL WITH EXPANDING CORNERS

Björn Lindgren

May 18, 1999

Department of Mechanics
Royal Institute of Technology

Abstract

A new low speed wind tunnel has been designed and built at the Department of Mechanics, KTH, under the leadership of professor Arne Johansson. The length of the test section is 4 m and the cross section area is 0.5×0.75 m^2. The tunnel is powered by 15 kW to give a maximum speed of 48 m/s with a normalized mean total pressure variation of $\pm 0.1\%$ in the cross-stream plane of the test section. The wind tunnel is built with expanding corners equipped with guide vanes designed to give very small losses and good flow quality. Measurements of the total pressure loss coefficient behind the first corner showed that the use of expanding corners is a good option to obtain a compact tunnel circuit with a minimum need for diffusers. The total pressure loss for the tunnel circuit is 0.46 of the dynamic pressure in the test section at a flow speed of 46 m/s. A relatively low noise level is also achieved by use of acoustic damping material in the sections surrounding the fan.

1 Introduction

At the Department of Mechanics, KTH, there were, until now, two low speed wind-tunnels operating. The larger of the two, named MTL after the late professor Mårten T Landahl, which initiated its construction, and **M**inimum **T**urbulence **L**evel, referring to the very good flow quality in its test section. This makes it suitable to use for basic research, such as transition and boundary layer studies, which requires a low disturbance level. Another central feature is a long test section enabling studies of high Reynolds number turbulent boundary layers. The test section measures 1.2×0.8 m^2 in cross-stream plane and the full tunnel length is about 25 m. The other low speed wind-tunnel is mainly used for student laboratory work. It has a rather small test section of 0.4×0.5 m^2 and rather poor flow quality. Some research projects have been carried out in this wind-tunnel over the years though.

The increase in number of students and research projects in recent years has lead to the need for more and better experimental resources, in the form of wind-tunnels, advanced measurement equipment etc. Therefore the planning for a new wind-tunnel started in 1994.

Initially the plan was to build an open wind-tunnel. The need for accurate temperature control and relatively high speeds turned the interest towards a closed circuit. During planning for reconstruction of the building in 1995, a sub-basement area was cleared and prepared to house the return section of the new wind-tunnel. This space is about 20 m in length, it has a width of 2 m and a height of 3 m. It is an ideal place to locate the return part of the wind-tunnel circuit, including the fan and motor, the frequency converter for the motor and the pump for the cooling water. New holes were made in the floor for the wind-tunnel circuit.

It became apparent that in order to reach desired goals regarding the dimensions of the test section a very compact design of the return circuit was needed. It was therefore decided to investigate the idea of using expanding corners. These experiments started in september 1995 as a masters thesis project by the present author. The results were so encouraging that it was decided to include the concept in the wind-tunnel design but more work was still needed to produce a new guide-vane optimized for the chosen expansion ratio. With a contraction ratio, CR, of 9 and with the expansion in the vertical plane entirely in the corners, the expansion ratio becomes 1.316 for each corner. With such corners, it was now possible to accommodate a test section with a length of 4 m and a cross section area of 0.5×0.75 m^2 in the available space.

The construction started in April 1996. The different parts of the wind tunnel, such as the driving unit, heat exchanger, screens, honeycomb and wooden parts, consisting of diffusers and corners, were delivered from various companies in Europe and the assembly of the parts was made by staff at the department. In October, 1998 the wind-tunnel was officially declared opened, but some finishing work and adjustments has taken place till the present day, (May 1999).

The first major research project in the tunnel has just started and concerns separated turbulent boundary layers. In this case the large degree of flexibility of the tunnel is utilized by using a specially designed test section.

A special feature of the tunnel is also a first diffuser downstream of the test section with variable diffuser angle to allow adaptation to different outlet areas of the test section. This gives a maximized freedom to vary e.g. the pressure gradient in the test section.

number	Part name
1	Test section
2	Diffuser
3	Corner
4	Driving unit
5	Heat exchanger
6	Screens & honeycomb
7	Stagnation chamber & contraction

Table 1: Numbering of the wind-tunnel parts in figure 1.

2 Wind-tunnel design

Much of the experience from the design of the MTL wind-tunnel was utilized for the present facility and some parts were given an identical design scaled-down to suit the present need. The MTL tunnel has a 7 m long test section and a cross section area of 1.2×0.8 m^2. The contraction ratio is 9 and the maximum speed is almost 70 m/s. It is also designed to have exceptional flow quality with a turbulence level in the test section of less than 0.03 % in the streamwise component and in the the vertical component it is below 0.06 %, [Johansson, 1992].

In order to also here achieve a good flow quality the elements of the stagnation chamber, the honeycomb and the screens were given a similar design for the present tunnel. The contraction shape is the same as for the MTL tunnel. Also the heat exchanger is of similar design and the test section aspect ratio is the same.

Major new features are the use of expanding corners, see section 2.4, and [Lindgren et al., 1998], (hereafter referred to as [LÖJ]) and the use of plane diffusers, one of which has a variable diffuser angle, see section 2.3. Faster and more elaborate temperature control and a more flexible and more versatile test section are also improvements from the MTL design.

To keep costs within a reasonable level we used standard industry equipment for the driving unit. This includes using a 12 blade axial fan with a 15 kW asynchronous AC motor, controlled with a frequency converter, rather than a DC motor, which earlier has been the most common choice in wind tunnel applications. This produces a top speed with empty test section of about 48 m/s. Acoustic damping material is only present in the silencers surrounding the fan.

The main construction material is plywood but plexiglass is used to improve visibility into the test section and the first diffuser. In the following, the different parts of the wind-tunnel will be described in detail. See figure 1 and table 1 for layout and numbering of the parts.

Note that the numbering of corners and diffusers start with the one

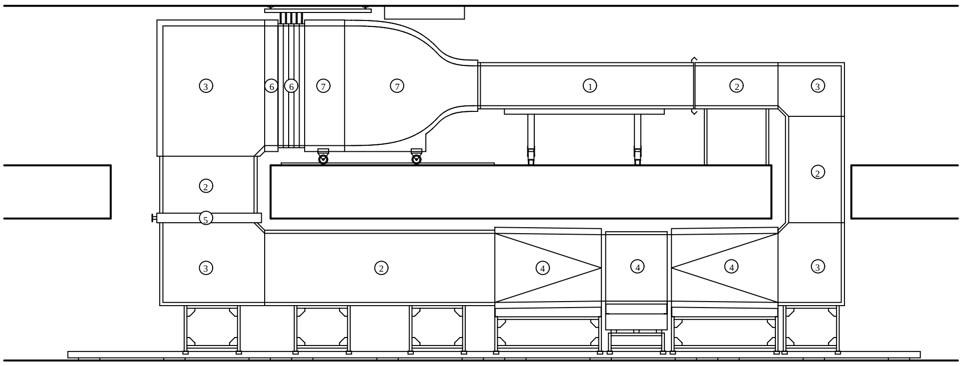

Figure 1: The wind-tunnel layout. The total circuit length is about 28 m.

closest to, and downstream of, the test section. this way of numbering is also used to number parts of the same kind, e.g. corners and diffusers.

2.1 Preliminary study of a closed circuit low speed wind-tunnel

In a closed circuit wind-tunnel, a change in dimension in any of its parts gives consequences for all other parts. Therefore a program that calculates the dimensions, the weights and the pressure losses of each part, together with the fan power and cooling power requirements was developed. It is also possible to use these data to optimize the choice of fan.

Figure 2 shows the total pressure variation through the wind-tunnel circuit. Note that the heat exchanger is located ahead of the third corner, unlike the position after the third corner, where it was finally located. See figure 1.

The friction coefficients for the tunnel circuit walls and formulas used to calculate the pressure loss of the tunnel circuit parts are based on empirical relations and they are not exact. The results are therefore only an estimate, but the calculated power factor of this wind-tunnel was 0.44 at a flow speed of 40 m/s which is not too far from the value achieved for the wind-tunnel that was finally built. The estimated losses in the wind-tunnel parts are shown in figure 3.

The power necessary to give a speed of 40 m/s is about 9 kW with the above estimate of the power factor. The cooling power required at 40 m/s was 13 kW, with a temperature difference between the room and the test section of 5° C.

2.2 Test section

The test section is the part with the smallest cross-section and thus the highest velocity. The specifications are set in terms of size, flow speed and

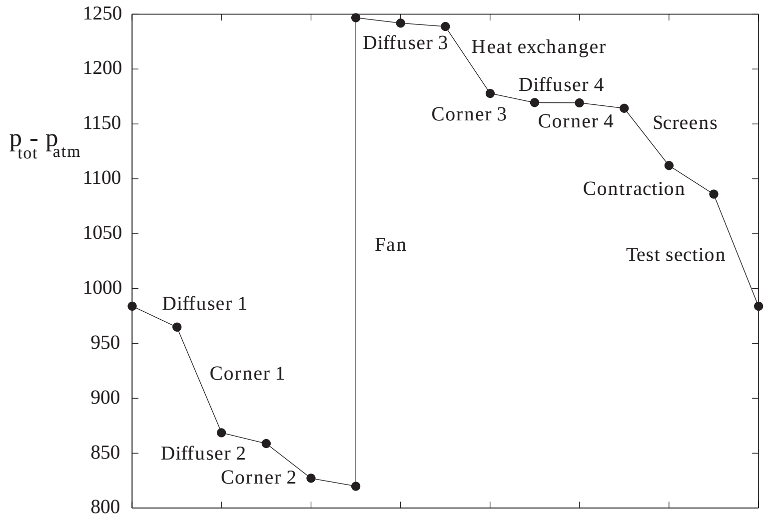

Figure 2: The total pressure variation through the prospected wind-tunnel at a speed in the test section of 40 m/s.

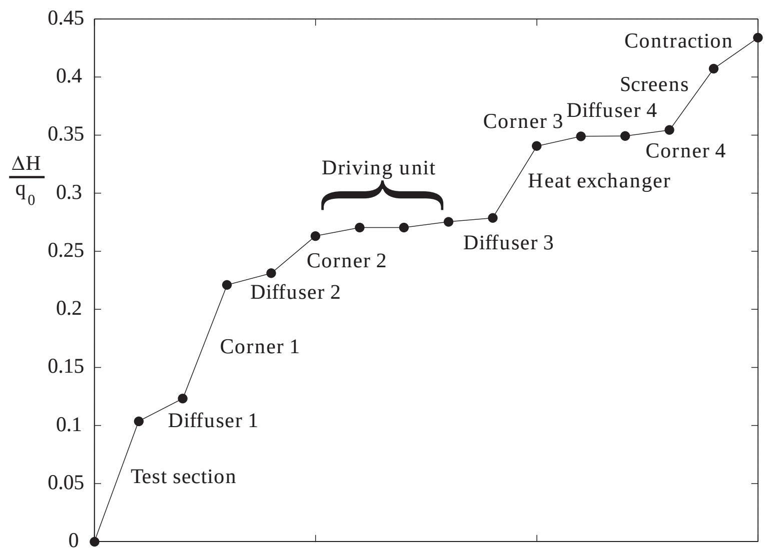

Figure 3: The cumulative total pressure loss at a test section speed of 40 m/s

flow quality in the test section. The other parts in the wind-tunnel are then designed so that the requirements for the test section are fulfilled.

Our aims where to construct a test section with similar characteristics, as the MTL wind-tunnel, but smaller. The test section was chosen to be 4 m long and have a cross section area of 0.50×0.75 m^2.

To enable the setting of the pressure gradient in the test section, one side wall is adjustable. For instance, to set a zero pressure gradient the cross section area can be increased downstream to compensate for boundary layer growth at the walls and measurement equipment installed in the test section. The reason for having only one adjustable wall is that the experience from the MTL wind-tunnel shows that it is very difficult and time consuming to adjust two opposite walls. We also opted for just two downstream positions with adjustable screws creating a spline shape of the plexiglass wall.

To maximize access to the interior of the test section both top and bottom walls are equipped with 6 hatches each and the side with the adjustable wall is removable to simplify the mounting of large measurement equipment, such as boundary layer plates and traversing systems. It is also possible to replace this wall with some other that may fit the current project better. One such example is the experiment on a separated turbulent boundary layer on a flat plate, that will be the first research project in the wind-tunnel. This project requires a large hump with suction and a special wall has been built for this purpose.

At the end of the test section there is a pressure equalizing slit that ensures that the static pressure in the test section is equal to the atmospheric pressure. The slit is filled with foam rubber to minimize noise.

2.3 Diffusers

A high contraction ratio, i.e. a large size of the stagnation chamber, is a key feature in obtaining a good flow quality and to minimize the pressure losses from the cooler, the screens and the honeycomb. This requires effective diffusers which is also necessary to minimize corner losses and friction losses on the wind-tunnel walls.

Since we are using expanding corners and all the expansion in the vertical plane is entirely done in the corners, the diffusers become two-dimensional, see figure 4. Two-dimensional plane diffusers are unfortunately not as efficient as three-dimensional diffusers in terms of pressure recovery. They are also more susceptible to separation, which means that the diffuser angle has to be smaller for two-dimensional diffusers than three-dimensional ones.

The geometry of a two-dimensional diffuser is shown in figure 4, where N is the diffuser length, $W1$ is the inlet width and θ is half the opening angle.

The risk for separation increases with increasing length of the diffuser. It is the influence from the boundary layers that makes them more prone to

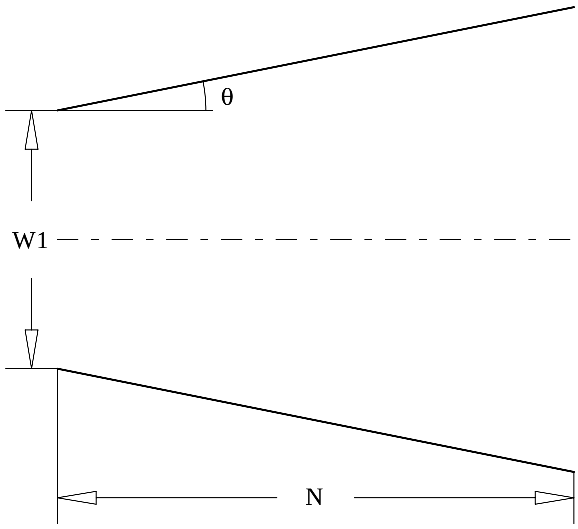

Figure 4: The geometry of 2D-diffusers.

separation. Ideally the shape of the diffuser should be concave with a larger diffuser angle at the beginning of the diffuser and a smaller at the end. Since it is more complex to manufacture such diffusers, ours have a constant diffuser angle. In figure 5, the risk of separation for two-dimensional diffusers is plotted against diffuser length. Our diffusers are also shown in the figure as filled circles.

Note that the line of maximum pressure recovery, (dashed line) lies slightly into the regime with separation. This is because the increase in pressure loss resulting from a small separation is smaller than the decrease in friction loss.

To get a good flow quality in the test section separation must be avoided and it is recommended that the diffusers should be well to the left of the separation line. In particular, diffuser 4 fulfills this requirement with a wide margin. To be able to use the full length of the test section for measurements the diffuser downstream of the test section has a variable diffuser angle. This means that the diffuser wall can match the adjustable wall in the test section section regardless of its position.

2.4 Corners

Partly because of space restrictions we decided to investigate the idea of using expanding corners to achieve a compact circuit design. Experiments on expanding corners go back as far as to the early 1930*s* but poor guide-vane design resulted in unfavorable test results and the idea was rejected. Some early experiments on expanding corners were made by [Collar, 1936], [Friedman and Westphal, 1952], [Kröber, 1932] and [Wolf, 1957].

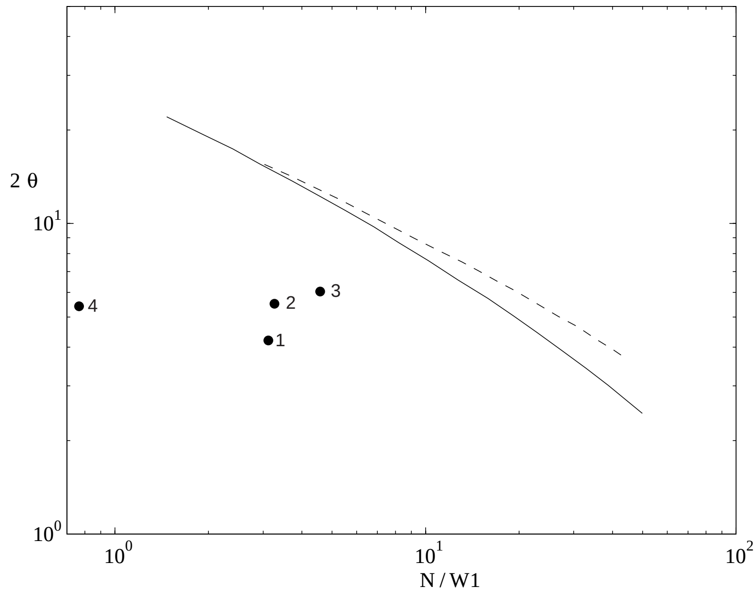

Figure 5: Solid line: separation of two-dimension diffusers. Dashed line: line of maximum pressure recovery. Filled circles: our diffusers numbered in the downstream direction from the test section.

Expanding corners have a larger outlet area than inlet area, see figure 6. The idea is to have expansion in the corners only in the vertical plane, resulting in the need for two-dimensional diffusers. The contraction ratio, CR, in the wind-tunnel is 9 and thus the expansion ratio of each of the four corners is $\sqrt[8]{9} \approx 1.32$. This is a large expansion and therefore it was important to validate the idea thoroughly before implementing it in the tunnel design, see [LÖJ].

The positioning of the guide-vanes in an expanding corner can be seen in figure 6, with the flow entering from the right and exiting to the bottom. In the ideal situation the flow will continue straight until it meets the guide vanes and then turn 90° in a distance equivalent to the guide vane cord, c. Experiments show that the flow tends to take a slight 'shortcut' in the corner at low chord Reynolds numbers.

The vanes in a cascade interact with each other, making it possible for each of them to carry a higher load than a single airfoil. Assuming that the turning angle is 90° the important parameters, see figure 7, are the guide vane chord, c, which is the distance from the leading edge to the trailing edge, the spacing , d, which is the spacing between the guide-vanes, and the expansion ratio, $e = \frac{h_2}{h_1}$, which is the ratio of the distance between the guide-vanes at the trailing edge and the leading edge, respectively.

Experiments on expanding corners with an expansion ratio, e, varying from 1 to $\frac{5}{3}$ using a scaled-down version of the MTL guide-vane showed that

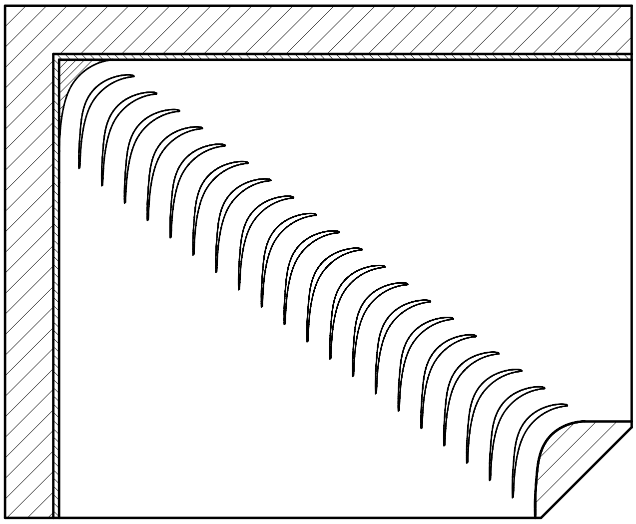

Figure 6: Corner number 1. The flow is from right to bottom.

for moderate expansion ratios, i.e. up to $\frac{4}{3}$, the flow was attached and the pressure-loss was still quite low compared to non-expanding corners with ordinary guide-vanes, see [LÖJ].

The guide-vanes are fixed in the first three corners, but in the fourth corner the angle of attack is adjustable about $\pm 3°$ to enable some optimization of the mean flow direction in the test section.

The use of expanding corners with present expansion ratio shortens the total wind-tunnel circuit length about 30 % for a given test section length. This is very important since it reduces both manufacturing and other costs. Another benefit is that the size of the fan becomes larger compared to the test section size for a wind-tunnel with expanding corners, since a large part of the total expansion is done in the first two corners. This reduces noise from the fan because a low rpm fan gives a low wing-tip speed. The rapid pressure recovery also lowers friction losses in the wind-tunnel circuit and therefore compensates for the somewhat larger total loss of an expanding corner compared to a non-expanding corner.

Low speed and thereby a low chord Reynolds number in the last corner may lead to some separation resulting in lower flow quality in the test section. The manufacturing of the guide vanes resulted in a larger camber than specified. This is compensated for by increasing the load on each vane, i.e. increasing the distance between the vanes, d, in the cascade. The increase in spacing between the vanes causes a slight separation near the trailing

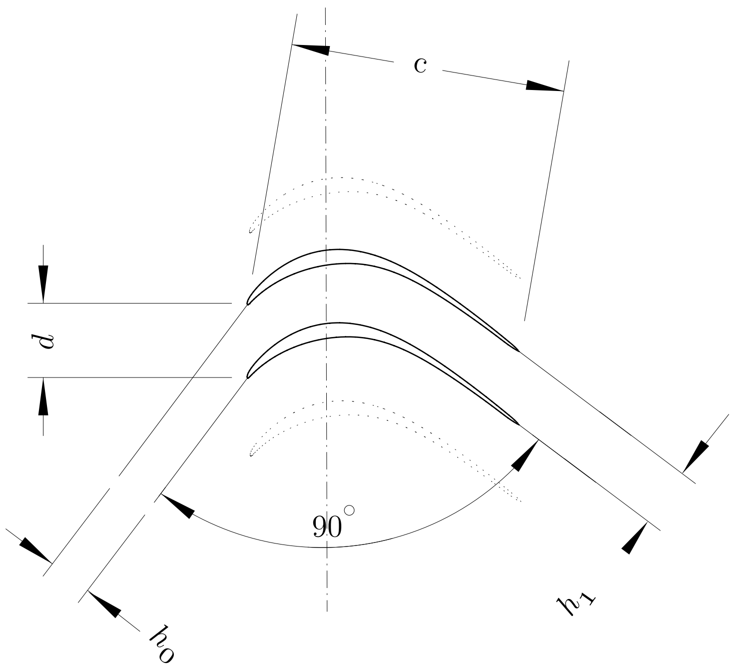

Figure 7: The geometry of an expanding cascade of guide-vanes.

edge of the guide-vane and the right outflow angle is thus achieved. This separation has also some effect on the flow quality but the larger spacing between the vanes reduces the total pressure drop in the corner, since fewer vanes lead to a reduction in friction loss.

2.5 Driving unit

The driving unit consists of the fan, motor and silencers. The fan is a standard industry fan with 12 blades and the motor is mounted axially right behind the fan. A cover surrounds the motor to improve flow quality. The fan is mounted on a 1000 kg heavy foundation which in turn is resting on 12 rubber dampers. The joints between the fan and the silencers are made of rubber cloth, ensuring that the fan induced vibrations do not spread through the wind-tunnel structure.

The angle of attack of the fan blades is 53°. This gives a fan efficiency of about 70 % and ensures that the blades never enter the stall region. At a nominal fan speed of 970 rpm the flow speed in the test section is about 45 m/s.

To save space the silencers also convert the cross section shape between rectangular and circular. A central body with elliptical nose is installed in the leading silencer and a conically shaped central body is installed in the trailing silencer to improve flow quality, see figure 8. The walls are also

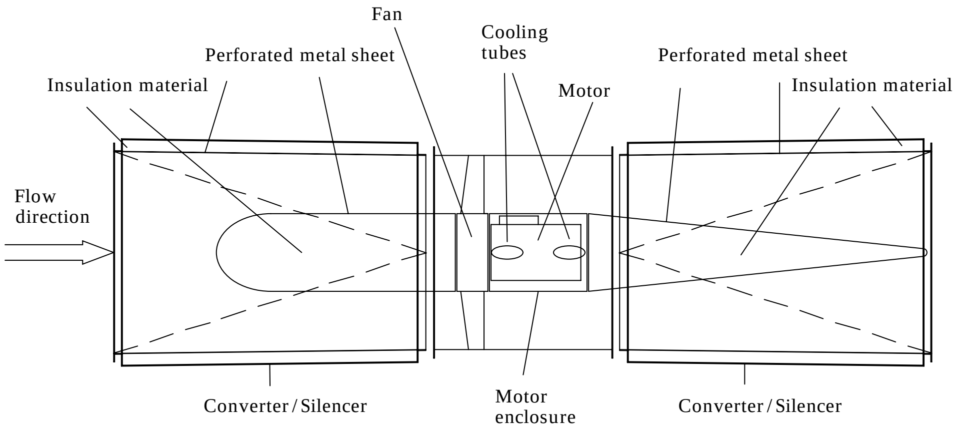

Figure 8: Plan of fan and silencers; flow from left to right.

filled with insulation material to reduce noise. Perforated plates cover the inside of the silencers and they separate the insulation material from the flow without blocking the sound from entering into the insulation material. This arrangement results in a very quiet wind-tunnel.

The motor is of asynchronous AC type and it is controlled with a frequency converter. It delivers 15 kW of power and has an efficiency factor of 0.88. The drawback with AC motors and frequency converters, is that the modulation of the frequency can interfere with the electronic measurement equipment. The advantage is that it is easy to operate, install and maintain.

The motor is cooled by air flowing through 2 elliptical pipes connecting the motor cover with the surrounding room and the air circulation is driven by a fan mounted on and driven by the motor.

2.6 Cooling system

The cooling system is built up by a primary and a secondary circuit of cooling water. In the primary circuit 10° C water from the main building air conditioning system flows. There is a high pressure and a low pressure side of this circuit and the pressure difference between the sides drives the flow through a valve, referred to as primary circuit valve, a throttle valve to increase the sensitivity of the primary circuit valve at low wind-tunnel speeds and a heat exchanger that transfer heat from the water in the secondary circuit to the primary circuit, see appendix A.6. Two PT-100 temperature sensors are attached to the pipes on either side of the heat exchanger to measure water temperatures.

In the secondary circuit, a multi step centrifugal pump driven is by a 1.1 kW AC motor. The pressure increase over the pump is 35 m H_2O at zero flow rate and is decreasing slightly with flow rate. The pump drives the flow through the air-water heat exchanger. This water is then mixed by the secondary circuit valve with water from a shunt pipe bypassing the air-water heat exchanger. In the shunt pipe there is a throttle valve so that the resistance through this pipe is the same as the resistance through the air-water heat exchanger, see appendix A.6.

The primary and secondary circuit valves are controlled by a current of $4-20$ mA and they are linear in flow rate with current input. The valves are very fast which is essential to give a fast and accurate temperature control.

The cooling of the air in a wind-tunnel is very important when measuring, especially when hot-wire anemometry is used. It is important to have low variations of temperature both in space and in time.

To achieve low variation in space, it is important that the air-water heat exchanger is designed to be as efficient as possible. This, however, means large pressure loss and high turbulence levels since the turbulent mixing of the flow increases heat transfer. Therefore it is important to place the heat exchanger both where the cross section area is as large as possible, to minimize pressure loss, and far away from the test section to minimize turbulence levels and mean temperature variations. It is unfortunately not possible to satisfy both these goals since the largest cross section area is in the stagnation chamber and it is very close to the test section, see figure 1. In many wind-tunnels the flow quality is, however, not so important and therefore the position of the heat exchanger is chosen to be in the stagnation chamber just upstream the screens. In this wind-tunnel it is placed on top of the third corner allowing the flow to go through the fourth diffuser and fourth corner before reaching the stagnation chamber, see figure 1.

It is also important to have a large flow rate through the heat exchanger to minimize the temperature difference between the water inlet and the water outlet. Of course this depends on how the water flows through the heat exchanger but the result will always be better with a large flow rate. Measurements of the flow rate through the heat exchanger and the water inlet and outlet temperatures have been performed, see section 3.3.

To achieve a steady temperature in the test section it is important to be able to control the flow rate accurately through the valve in the primary circuit instantly and to have short distance between the heat exchangers, minimizing time lag. Without using the shunt valve the time lag in the wind-tunnel is about 20 s at a test section flow speed of 25 m/s. The valve in the secondary circuit can be used to shut off the flow to the air-water heat exchanger if there is a rapid change in temperature or speed in the wind-tunnel. When the PI-control loop is used the valve in the secondary circuit is, however, always fully open.

2.7 Screens and honeycomb

An important part of the turbulence reduction package in the wind-tunnel is the section containing the honeycomb and the screens. They reduce the turbulence by breaking it down to smaller and smaller scales. The interaction between the turbulence generated by the screen itself and the original turbulence leads to a rapid decrease in intensity downstream of the screen. It is important that the mesh size, M, of the screen is substantially smaller than the macro scale of the incoming turbulence, see figure 9. Therefore the turbulence level can be reduced further by using a series of screens with finer and finer mesh size. This cascade effect is achieved in the wind-tunnel by five screens with consecutively smaller mesh sizes, see table 2.

The reduction of the turbulence is not the same in the streamwise component as in the cross-stream components. Especially for screens which are sub-critical, i.e. with the wire-diameter Reynolds number less than 45, the reduction in the streamwise component is much higher,
see [Groth and Johansson, 1988].

Sub-critical screens also give a much larger reduction of the turbulence level, although to a price of a pressure loss that is several times higher than for a super-critical screen.

The honeycomb and the screens also reduce flow deviation angles. They work in the same way as a surface with a refractive index, $\frac{1}{\alpha}$, (between 0 and 1). The relation of the outflow angle, ϕ, to the inflow angle, θ, for small angles can be written as, (figure 10)

$$\phi = \alpha\theta. \tag{1}$$

Since α is between 0 and 1 it follows that the flow angle will be reduced when it passes a screen or the honeycomb. Empirically it has been found that α can be related to the pressure loss coefficient, K_0, in the following way,

$$\alpha = \frac{1.1}{\sqrt{1+K_0}}. \tag{2}$$

The pressure loss coefficient is determined by the solidity of the screen and the Reynolds number based on the wire diameter, d. The solidity is defined as $1-\beta$ where β, the porosity of the screen, in turn is defined as

$$\beta = \left(1 - \frac{d}{M}\right)^2, \tag{3}$$

where d is the wire diameter and M is the mesh size, see figure 9. The pressure loss coefficient, K_0, can be approximated by the following relation derived by [Laws and Livesey, 1978]

$$K_0 = f\left(Re_d\right)\frac{1-\beta^2}{\beta^2} \tag{4}$$

where $f\left(Re_d\right)$ is a function depending on the wire-diameter Reynolds number. If a friction less flow is assumed, $\frac{1-\beta^2}{\beta^2}$ is the relative pressure difference

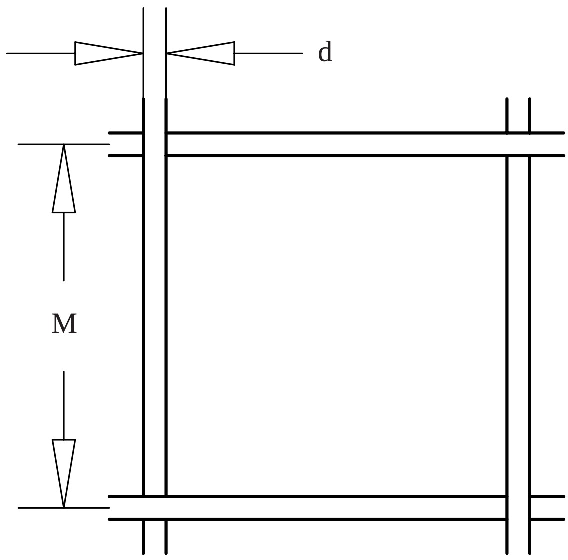

Figure 9: Definitions of mesh size, M, and wire diameter, d, of a screen.

between a position upstream and one in the plane of the screen. The recovered pressure downstream of the screen is $1 - f$.

For high Reynolds numbers, i.e. Reynolds numbers above 100 the function f is almost constant and for solidities in the interval $0.3 - 0.4$ the value is approximately 0.5. In this region the flow is super-critical, i.e. small-scale turbulence is generated by the wires of the screen. For Reynolds numbers lower than 45 the function, f, increases rapidly with decreasing Reynolds number. In this region the flow over the screen is laminar (subcritical). It is recommended to choose screens with large enough wire diameter to avoid the laminar region in order to get low pressure loss, see [Groth and Johansson, 1988].

The honeycomb and screens reduce the mean flow variation over the cross section. To achieve this they need to have a porosity, β, larger than 55 %, see table 2. With a porosity less than 55 % the jets from the openings in the screen will coalesce with a large variation of the mean velocity as a result. This phenomenon is called jet-collapse.

If jet-collapse is avoided, the reduction of the mean flow variation can be estimated by the following expression, derived by [Taylor and Batchelor, 1949]

$$\frac{\Delta u_2}{\Delta u_1} = \frac{1 + \alpha - \alpha K_0}{1 + \alpha + K_0} \tag{5}$$

where index 1 refers to a position upstream of the screen and index 2 refers to a position downstream of the screen.

If a screen is designed to have a pressure loss of $K_0 = 1 + \frac{1}{\alpha}$ the mean flow variations would be completely eliminated. Unfortunately this will lead to a

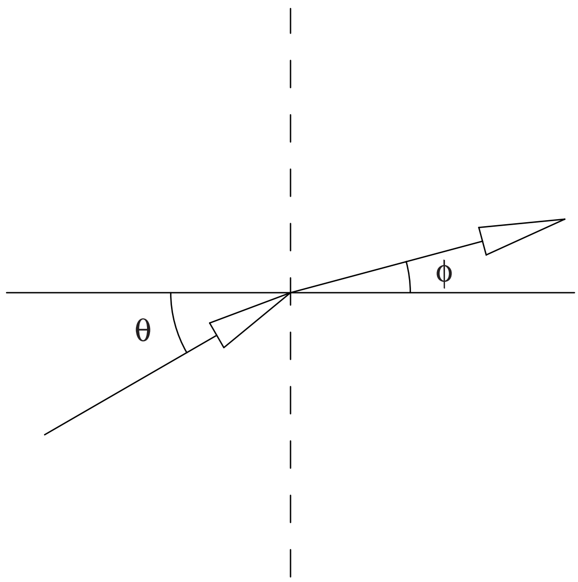

Figure 10: In- and outflow deviation angle passing a screen, here depicted as a dashed line.

Screen	d $[mm]$	M $[mm]$	β	Re_d	K_0	f
1	0.71	3.2	0.61	210	0.80	0.50
2	0.56	2.4	0.58	165	0.99	0.55
3	0.56	2.4	0.58	165	0.99	0.55
4	0.16	0.7	0.61	47	1.71	0.75
5	0.16	0.7	0.61	47	1.71	0.75
honeycomb	0.1	6.35	0.97	29	-	-

Table 2: Data for the screens and the honeycomb used in the new tunnel at a test section flow speed of 40 m/s.

screen where the porosity, β, becomes 0.37, which is way below the stipulated 0.55 to avoid jet-collapse.

The similarities between a honeycomb and a screen may suggest that it would be more convenient to replace it with one or more screens. A honeycomb is very fragile because of the thin foil it is made of, see table 2, and skewness of the cells can lead to varying amount of blockage over different parts of the cross section, resulting in mean flow variations. The advantage is that α for a honeycomb is substantially smaller than for a screen. We decided to use a honeycomb in this wind-tunnel. If problems with the honeycomb would arise it can easily be removed.

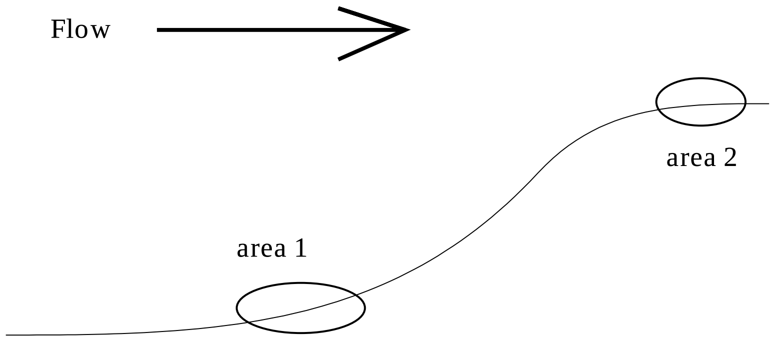

Figure 11: The areas of the contraction that are most subjected to separation

2.8 Stagnation chamber and contraction

The last wind-tunnel parts the flow passes before it enters the test section are the stagnation chamber followed by the contraction. The stagnation chamber, is also called settling chamber, which is a more appropriate name since it describes its purpose. The purpose of the stagnation chamber is thus to allow the flow to settle or relax. When the flow has passed the honeycomb and screens the turbulence is very anisotropic, because the turbulence reduction in these parts is not equal in the streamwise and in the cross-stream directions. Therefore it is important to let the flow relax and reach an isotropic state before it enters the contraction where it will be submitted to large strain again. The higher the contraction ratio the higher the strain and anisotropy.

The shape of the contraction is very important. It is absolutely crucial that separation of the boundary layers is avoided. There are two regions in the contraction that are sensitive, see figure 11.

The first is the concave region in the beginning of the contraction. It is important to minimize the pressure gradient here. Therefore this part of the contraction has to be as long as possible. A separation in this area will not be steady but it will move back and forth in the streamwise direction. This would ruin the flow quality in the test section.

The second part which is sensitive to separation is in the convex part close to the exit of the contraction. This separation is easier to prevent. By attaching trip tape on the contraction walls close to the exit the thin laminar boundary layers will be transformed to turbulent boundary layers which are more resistant to separation.

The contraction shape used in this wind-tunnel is the same as in the MTL wind-tunnel. It has been carefully designed and tested to give good flow quality and the low turbulence level in the MTL wind-tunnel is proof of its quality, see figure 12.

The function describing the shape of the contraction is

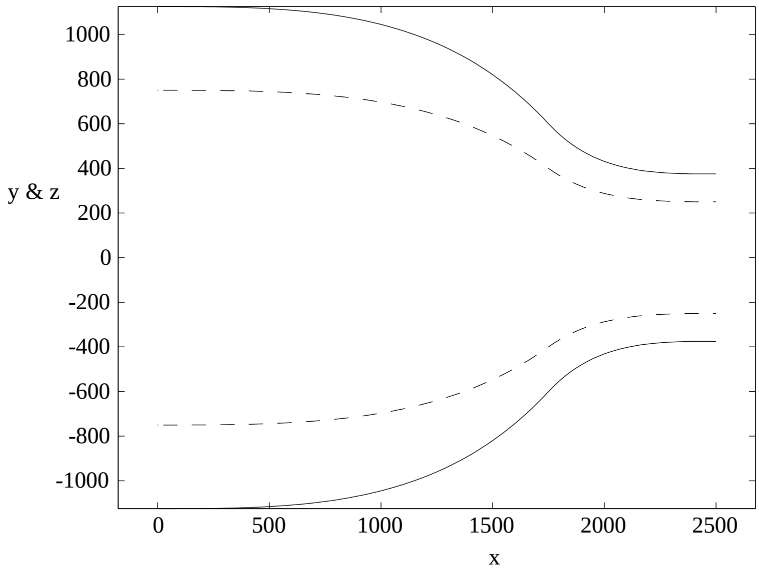

Figure 12: The shape of the contraction. Solid line: side view. Dashed line: top view. The flow is from left to right.

$$y = A\left(\sinh\left(B\frac{x}{L}\right) - B\frac{x}{L}\right), \qquad \frac{x}{L} \leq 0.7 \tag{6}$$

$$y = 1.0 - C\left(\sinh\left(D\left(1-\frac{x}{L}\right)\right) - D\left(1-\frac{x}{L}\right)\right), \qquad \frac{x}{L} > 0.7 \tag{7}$$

where $A = 0.205819$, $B = 3.52918$, $C = 0.08819$ and $D = 8.23523$. x is the downstream coordinate and L is the contraction length. The vertical and horizontal shapes, respectively, are given by

$$V = \pm h\left(\frac{\sqrt{CR}}{2} - y\left(\frac{x}{L}\right)\right) \tag{8}$$

$$H = \pm b\left(\frac{\sqrt{CR}}{2} - y\left(\frac{x}{L}\right)\right) \tag{9}$$

where h is the test section height, b is the test section width, CR is the contraction ratio and L is the contraction length. The length of the contraction is here 2.5 m and the contraction ratio is 9.

Turbulence reduction in the contraction is, as mentioned above, not equal in the streamwise and cross-stream directions. In the streamwise direction the reduction is much larger but it is substantial in all directions.

The reduction in mean velocity variation are in streamwise and cross-stream directions

$$\frac{\Delta u_1}{U_1} = \frac{\Delta u_0}{CR^2 U_0} \tag{10}$$

$$\frac{\Delta v_1}{U_1} = \frac{\Delta v_0}{\sqrt{CR} U_0} \tag{11}$$

respectively, where U is the mean flow velocity, Δu and Δv is the velocity variations in the streamwise and cross-stream directions with subscripts 0 for the inlet and 1 for the outlet. Note that the streamwise component is reduced 81 times for a contraction ratio, CR, of 9. This can also be used as a (not very accurate) first approximation of the reduction in turbulence intensities. To accurately predict the damping of the turbulence intensities we need to use realistic turbulence model equations. The main conclusion is valid also for the intensities, namely that the contraction is the single most important element for the flow quality.

2.9 Wind-tunnel control system

One important aspect of an experimental apparatus such as a wind-tunnel is the way it is operated. It is very convenient to be able to control everything, such as fan speed, cooling pump and valves from a single computer. This is achieved through the National Instruments Field Point system. The Field Point system used here consists of four terminals, which can later be complemented, if new needs arise in the future. It consists of a communication terminal, a terminal for analog output, a terminal for discrete output and a terminal for measuring temperatures, see figure 13.

FP-1000 is the communication terminal that communicates with the computer, used for controlling the wind-tunnel, through a serial RS-232 port. It contains a flash memory saving the settings for the next start-up. It also distributes the power necessary to operate the other terminals.

FP-AO-200 is a 12 bit analog output and it can deliver a current between $0 - 20.5$ mA or $3.5 - 20.5$ mA for 8 channels simultaneously. This terminal is used to control the valves in the cooling system, see appendix A.6, and the fan speed.

FP-DO-400, the discrete output, is an 8 channel terminal with an output of 24 V and a maximum current of 2 A for on and 0 V for off. This terminal is used for turning on the fan and the pump.

FP-RTD-122 is a terminal that sends out small currents intermittently so that the resistance of a PT-100 temperature sensor can be measured. It has a built-in three-wire compensation to eliminate wire resistance and a filter against $50 - 60$ Hz noise. The resolution is 16 bit and the number of channels is 8.

The computer connected to the Field Point system communicates through LabView Optomux serial commands. It also serves as a slave to some other

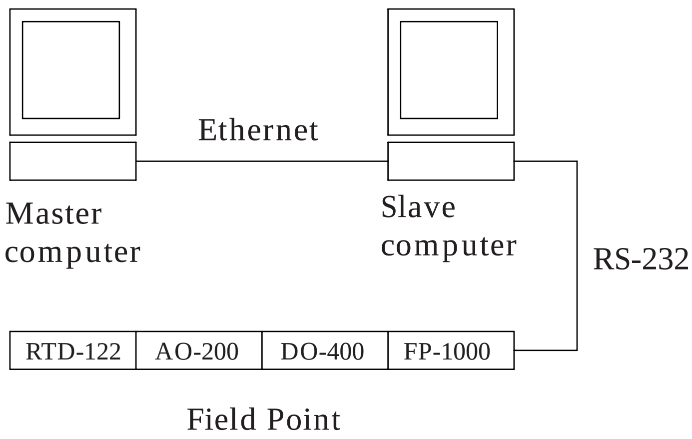

Figure 13: The communication between the computers and the Field Point system.

computer that may be used for the measurements. This communication is through the ethernet which means that the master computer can be located anywhere. The advantage of this system is that the slave computer is not contaminated with different users programs, files and boards for data acquisition and traversing, providing for a more problem-free operation. It also gives the users the possibility to bring their own computer for the measurements and thus the programs on that computer can be developed and tested without needing direct access to the tunnel.

A cabinet on the wall behind the forth corner contains, besides the Field Point system, other electrical devices such as relays, transformers and switches, needed to operate the wind-tunnel. There are also two safety stops to guarantee safe operation. For the electrical scheme see appendix A.7.

2.10 Traversing equipment

To be able to measure turbulence statistics over a cross flow plane a traversing arm was built. It works in almost the same way as a human arm with one joint in the wall, (shoulder), one joint in the center, (elbow) and one joint at the end, (wrist). The difference is that the arm can only move in the cross flow plane since all the axes of rotation are in the flow direction. The reason for having a joint at the end of the arm, which is not necessary to reach a certain position in the cross section, is that the spear attached to this joint must be able to rotate to keep the probes at the end of it horizontal. A sketch of the arm from the front can be seen in figure 15 and photo 14 shows the arm from the side.

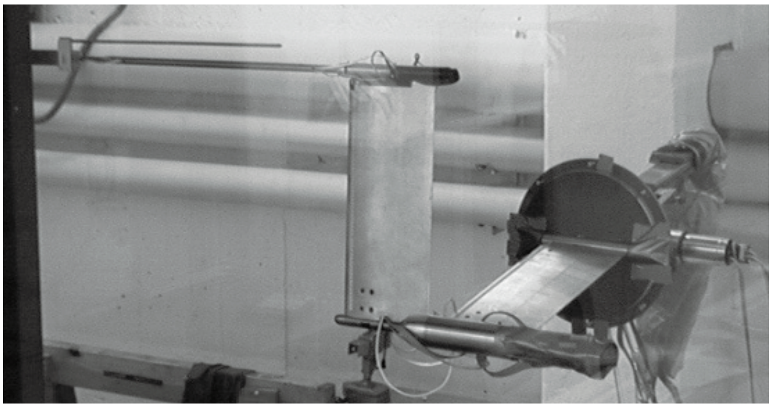

Figure 14: The traversing arm used for measurements in the test section.

joint	torque Nm	gear	encoder
1	10	478:1	360
2	6.75	531:1	500
3	0.45	1621:1	16

Table 3: The maximum torque, gear and encoder used for the traversing equipment

All joints are equipped with servo motors and encoders, see table 3, so that the traversing can be done automatically. The necessity for using small motors, so that the blockage of the flow in the test section does not become too large, requires large reduction gears to increase maximum torque. This also increases the accuracy. However, the accuracy is somewhat limited because of the play that comes with large reduction gears.

There are also errors introduced in the initialization of the arm position. This initialization is made by taking a photo with a digital camera of the position of the arms relative to a plummet, see figure 16. By analyzing the photograph and calculating the angles between the plummet and the arms the position of the probe in the cross flow plane can be calculated. However, the accuracy of the traversing arm is not so crucial since the measuring points are separated by, typically, a few centimeters.

The traversing arm is equipped with two pressure tubes and four wires. This means that it is possible to use Pitot and Prandtl tubes as well as a flow angle pressure probe. It is also possible to use single and cross-wire hot-wire anemometry and it is possible to use a PT-100 temperature sensor to measure temperature differences in the cross section. The temperature sensor needs three wires to compensate for wire resistance.

The tubes and the wires together with cables for motors are running inside the arms out of the test section for minimum flow disturbances. The

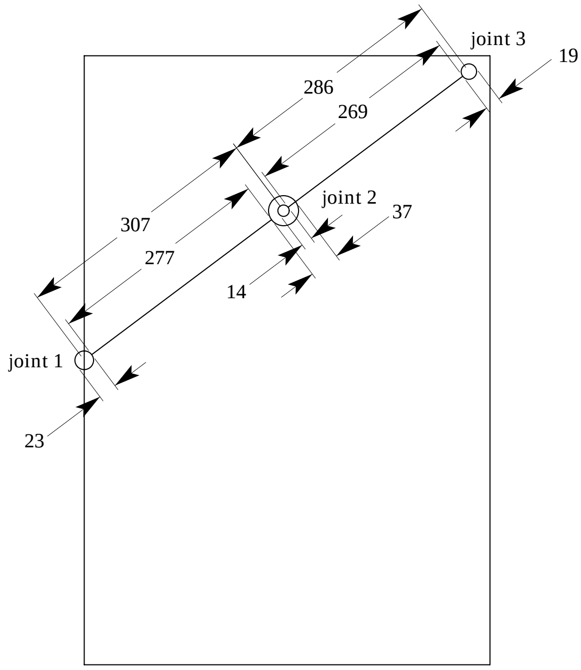

Figure 15: A sketch of the traversing arm used for measurements in the test section; front view.

arms have a symmetric wing shape and are made of extruded aluminum. Trip tape has been attached near the leading edge on both sides of the arms to eliminate the noise and vibrations caused by interaction of the wake from the traversing equipment and the first corner guide-vanes.

Figure 16: The positions of the arms at initialization. Note the plummet which is the white line to the right in the photograph.

3 Measurements

The measurements over the cross section in the test section are made 0.25 m from the entrance. The probes can be traversed across the entire cross section but no measurements close to the walls were performed since the important part of the flow region is away from the wall boundary layers.

The measurements included in this report are pressure measurements to investigate the mean flow angle variation and the total pressure variation in the cross section. The temperature variation in time and the behavior of the PI-regulator are also examined, along with measurements of the temperature variation over the cross section. The flow-rate through the heat exchanger is measured, so that the cooling power can be estimated and thereby contribute to a more efficient cooling control loop with less temperature variation in the test section. Noise levels outside the test section and the driving unit are measured. The pressure build-up over the fan was measured to calculate the power factor. Furthermore, the distribution of total pressure behind the first corner with an empty test section has been performed to compare the behavior of this expanding corner with the experiments and calculations performed with guide-vanes for non-expanding corners and the calculations for the optimized guide-vane now used in this wind-tunnel, see [LÖJ].

The flow speed in the test section is around 25 m/s for most measurements except when the fan speed is varied. This velocity is chosen because it is the intended operation speed for most of the experiments that will take place in the wind-tunnel.

In the future more measurements including single and cross-wire constant temperature anemometry will be carried out to complete the calibration of the new wind-tunnel.

3.1 Flow angle variations in the test section

One important flow quality feature is the flow angle variation in the test section. By measuring this variation it is possible to spot vortices that may travel along the test section interfering with e.g. cross-wire measurements. The difficulty with measuring flow angle deviations is that the angles are so small that a very sensitive probe is needed. Therefore a special pressure probe shown in figure 17 is used. This probe is a flat plate with two pressure holes, one on each side of the plate. The idea is to register the pressure difference between the two holes that appears when the stagnation point moves on the rounded leading edge. To accentuate the pressure difference a 45° V-shape is cut into the leading edge (figure 17).

The probe has been calibrated in the MTL wind-tunnel at the same flow speed as the one used in the present measurements. The calibration yields a linear relation between the pressure difference and the deviation angle for moderate angles of attack. The sensitivity is 21.23 Pa/degree, (figure 18).

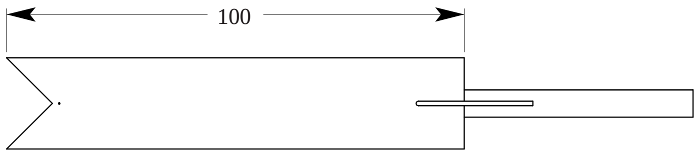

Figure 17: The pressure probe used for flow deviation measurements. Note the pressure hole at the bottom of the V shape.

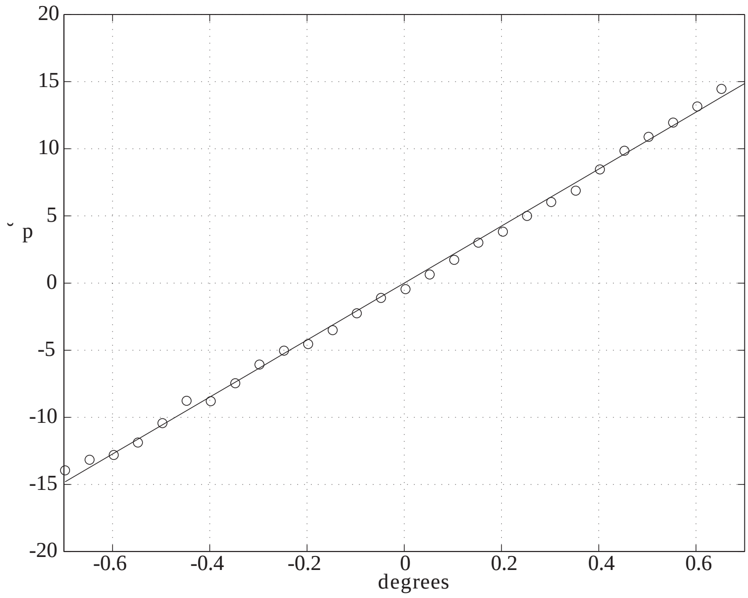

Figure 18: The calibration curve of pressure difference versus deviation angle

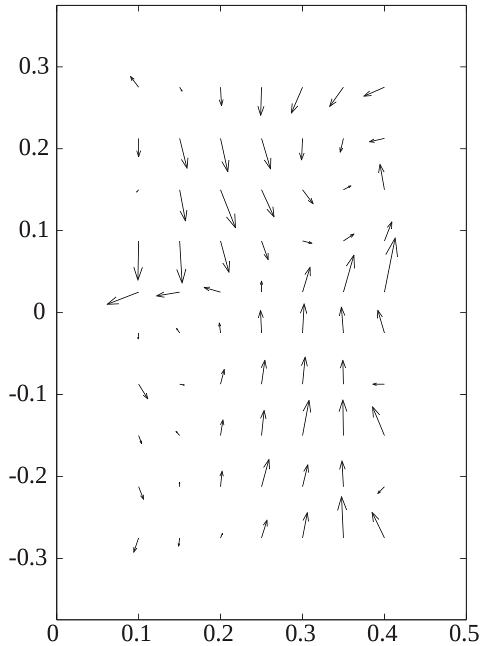

Figure 19: The flow deviation in the test section. Largest arrow equals 0.1°.

The results from the measurement showed a flow angle variation of less than 0.1°, see figure 19. This is of the same order of magnitude as in the MTL tunnel, see [Johansson, 1992]. However, absolute value and direction of the arrows are very sensitive to angular errors in the traversing equipment that may be caused in the manufacturing or by lift on the wing shaped arms. Studies showed that there are no variation caused by lift but there are errors from the manufacturing. Some compensation has been made for this error. The lift on the wings also causes deviations in the flow angle in front of the wings. The probe is mounted 0.5 m in front of the traversing arms. This should be enough if the lift on the arms is small.

3.2 Mean total pressure variations in the test section

One of the most important factors regarding the quality of a wind-tunnel is the uniformity of the flow speed over the cross section in the test section. This is done by measuring the variation of the total pressure. A good reference pressure is the total pressure somewhere in the stagnation chamber. The pressure measured in the experiment was the difference between this reference total pressure and the total pressure in the test section. Because of the total pressure loss in the contraction it is convenient to subtract the measured total pressure difference with its mean value. Finally, we normalize with the dynamic pressure in the test section. The final expression

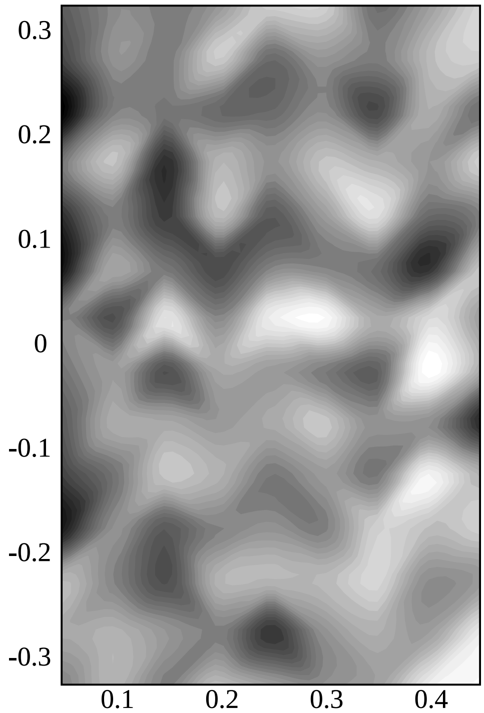

Figure 20: The variation of total pressure in the test section. Black represents a minimum level of -0.1 % and white a maximum level of $+0.1$ %.

reads

$$\frac{\Delta p_{tot}}{q_{test}} = \frac{p_{tot,test} - p_{tot,stag} - \overline{p_{tot,test} - p_{tot,stag}}}{q_{test}} \tag{12}$$

where $p_{tot,test}$ is the total pressure in the test section, $p_{tot,stag}$ is the total pressure in the stagnation chamber and q_{test} is the dynamic pressure in the test section.

To avoid influence from the growing boundary layers on the test section walls and other disturbances, such as non-smooth edges between walls and hatches, the measurements took place at a downstream position from the beginning of the wind-tunnel of about 0.25 m.

The dynamic pressure variation gives an indication of the performance of the screens, the honeycomb and the guide-vanes in the forth corner as well as the contraction. Any defects or bad design would show up clearly in the measurements. The result at a flow speed of about 25 m/s is shown in figure 20.

The results are comparable to the ones obtained in the MTL wind-tunnel, see [Johansson, 1992], with a peak to peak variation of the total pressure of ± 0.1 % which corresponds to a velocity variation of ± 0.05 %. As seen in figure 20 there are a few spots with low speed covering a rather small area. Therefore the standard deviation might be a suitable measure of the variation encountered in the area where measurements usually take place. The standard deviation is 0.03 %.

It is interesting to note that there seems to be some low and high speed streaks running from left to right. This could perhaps be a trace of the wakes from the guide-vanes. The test section is rotated 90° compared to the MTL wind-tunnel. This means that a boundary layer plate will be mounted vertically rather than horizontally and the spanwise variation of the total pressure will, as a result of this, be somewhat larger than in the MTL wind-tunnel.

Some of the areas of lower total pressure seen in the figure may be a consequence of the variation over the cross section of the skewness of the honeycomb cells. The skewness of the cells increases the blockage of the flow leading to lower speed and consequently to lower total pressure.

3.3 Temperature measurements

Measurements of cooling capacity showed that the water flow through the air-water heat exchanger was very small. By measuring the power input into the wind-tunnel through the fan and measuring the inflow and outflow water temperatures the flow rate can be estimated by the expression

$$Q = \frac{P}{c_p \rho \Delta T} \tag{13}$$

where Q is the volume flux, P is the power input, c_p is the specific heat coefficient and ΔT is the temperature difference between inflow and outflow. The flow rate was found to be about 1.5 m^3/h. Using equation 13 and estimating the total pressure loss in the piping system the pressure increase over the pump was estimated to be around 3 m H_2O. This was later confirmed by a direct pressure measurement over the pump. The problem with a low flow rate of the cooling medium is that the temperature difference over the heat exchanger will result in large temperature variations over the cross section area of the test section. In this case the temperature difference over the heat exchanger was about 6° C at a wind-tunnel speed of 25 m/s, which is too much.

A larger pump delivering 35 m H_2O was installed together with 1 inch piping rater than the previous $\frac{1}{2}$ inch. A larger flow control valve and a venturi flow meter was also installed. The flow through a venturi pipe can be calculated as

$$Q = c_d A_1 A_2 \sqrt{\frac{2\Delta p}{\rho(A_1^2 - A_2^2)}} \tag{14}$$

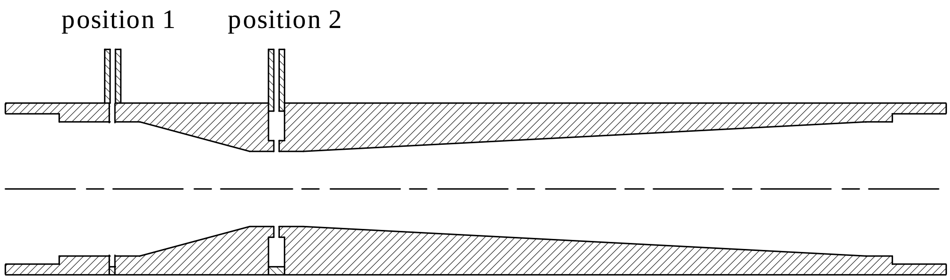

Figure 21: The venturi pipe for measuring the flow in the cooling system

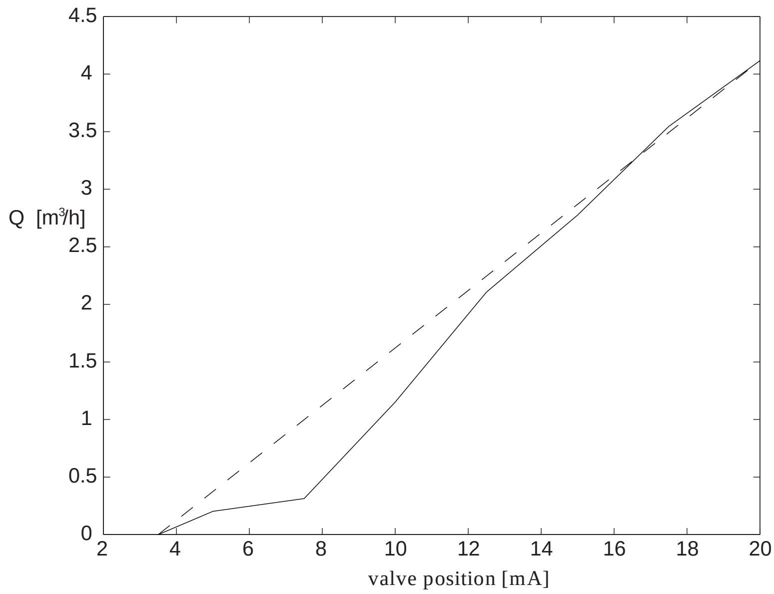

Figure 22: Flow rate versus control current, (3.5-20 mA).

where $c_d = 0.98$ is friction loss, A_1 and A_2 is the pipe area at position 1 and 2 respectively, (figure 21). Δp is the pressure difference between positions 1 and 2 and ρ is the density of the flowing medium. The flow was now about 4.1 m^3/h and the temperature difference between inflowing and outflowing water is less than 1° C at a test section speed of 25 m/s.

The flow rate through the air-water heat exchanger varies with valve control current as in figure 22. The solid line is the values measured by the pressure difference over the venturi pipe. The flow through the valve should be linear, dashed line. The reason for deviation could be that the pressure drop in the shunt pipe is too low compared to the rest of the circuit. The inaccuracy of the pressure sensor at low pressure differences may also contribute to the deviation.

The temperature in the test section is very steady. The variation is

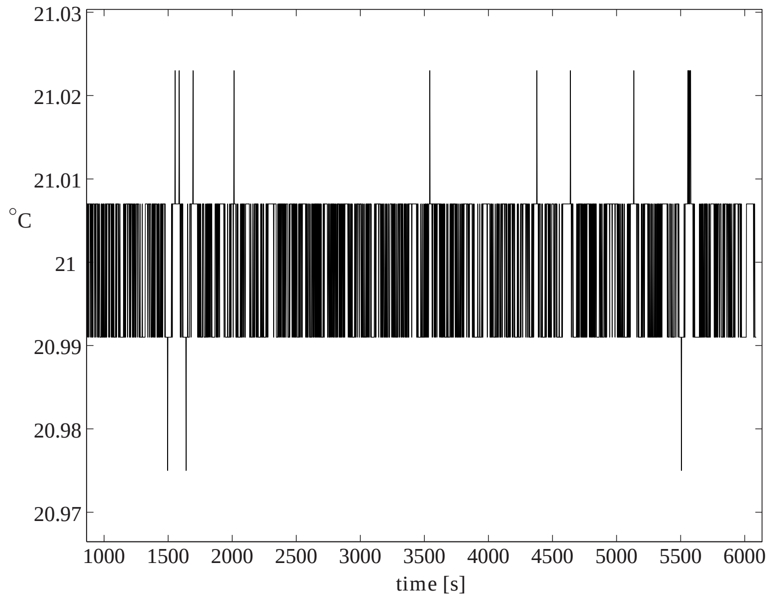

Figure 23: Temperature in the test section versus time.

about $\pm 0.03°$ C at a flow speed of 25 m/s and a difference between ambient temperature and test section temperature of 2° C (figure 23). The 16 bit AD converter gives a resolution of 0.016° C per bit.

The temperature control algorithm used in this measurement is of PI type with the constants $K = 7.65$ and $T_I = 67$. The constants where derived using the Ziegler-Nichols method, The PI control algorithm can be written in discrete form as

$$u_n = K \left(e_n + \frac{\Delta t}{T_I} \sum_{k=0}^{n} e_k \right) \tag{15}$$

where u_n is the control signal output, Δt is the time between samples and $e_n = T_{set} - T(t)$ is the error where T_{set} is the desired value and $T(t)$ is the actual temperature. This way of implementing the algorithm is good as long as the control signal does not reach its limits. If this happens the integrating part becomes very large and it takes a long time until it decreases to a normal level. This is called the saturation problem and it can be dealt with by rewriting the output, u_n on the form $u_n = u_{n-1} + \Delta u$ with

$$\Delta u_n = K \left(e_n - e_{n-1} + \frac{\Delta t}{T_I} e_n \right). \tag{16}$$

The damping time is about 850 seconds and the overshoot 0.7° C (figure 24). This can be improved by using more advanced control algorithms. Such algorithms will be implemented in the future.

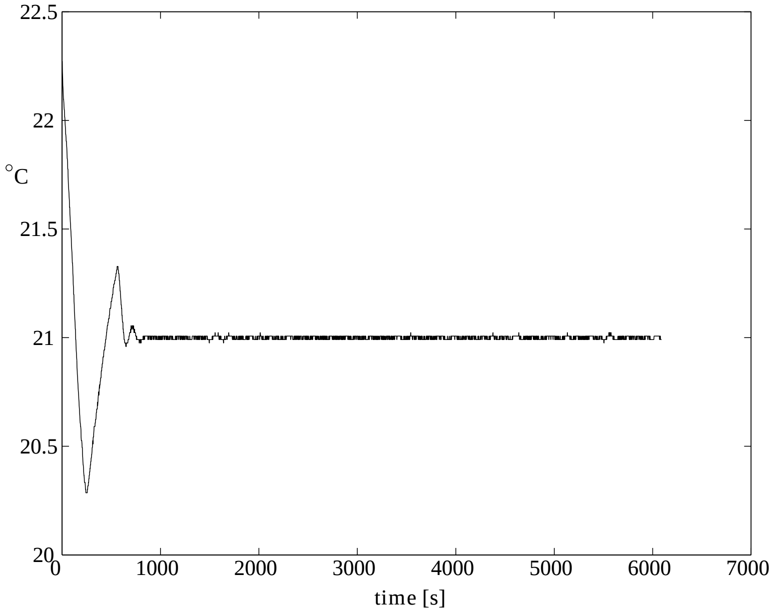

Figure 24: Temperature in the test section versus time.

Measurements of the variation of temperature in the test section cross section area, at a flow speed of 25 m/s and a temperature difference between the room and the test section of 2° C, showed that the differences were small, ±0.07° C but with generally higher temperatures at the bottom and lower at the top of the test section (figure 25). There were also a slight difference in temperature of the two sides of the wind-tunnel. This could be explained by the fact that the inlet of cooling water is at the top right corner of the figure and the outlet at the top left. The difference in cooling water temperature between the outlet and inlet was about 0.2° C.

One must also bare in mind that the temperature in the test section also varies in time. This variation is in the order of magnitude of 0.03° C and therefore figure 25 can only be seen in a qualitatively way.

3.4 Estimation of the power factor

The original setup showed considerable deficiencies with fan blade angle of attack, α, variations of $\pm 1°$ and a mean angle of attack of 63°, see table 4. This is very close to the stall region. At high angles of attack the fan efficiency was as low as $60 - 65$ %. The velocity was varying considerably in space and time in the test section and a low frequency noise could be heard at all speeds. The fan was also subjected to rather large vibrations. As seen in table 4, the preset blades with higher and lower angle of attack are gathered together. This leads to aerodynamic imbalances with resulting

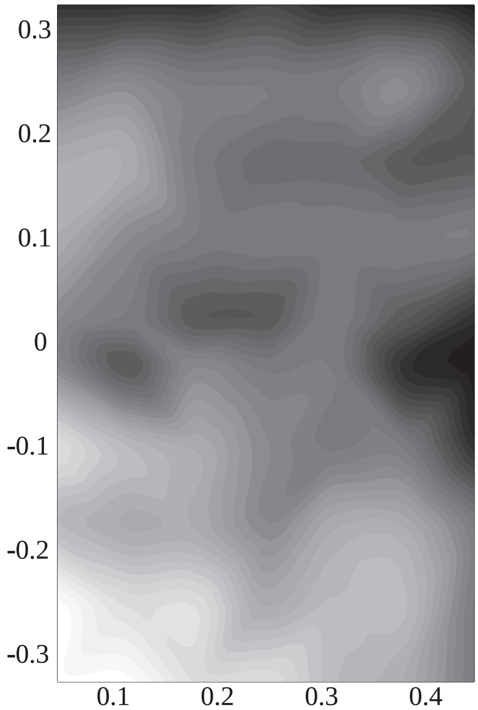

Figure 25: The temperature variation over the cross section of the test section. Black is $-0.06°$ C and white is $0.07°$ C.

blade no.	1	2	3	4	5	6	7	8	9	10	11	12
α_{preset}	63	64	64	64	62	63	63	63	62	62	64	64
$\alpha_{present}$	53	53	53	53	53	53	53	53	53	53	53	53

Table 4: Fan blade angle of attack, before and after adjustments.

pressure pulses and vibrations. The solution was to reduce the angle of attack to 53° and thus locating the working point of the fan close to the point with maximum efficiency.

By measuring the pressure increase over the fan, or the power input and the speed in the test section it is possible to calculate the power factor, λ, which is a measure of the resistance in the wind-tunnel circuit. It is defined as,

$$\lambda = \frac{\Delta p_{tot}}{\eta_{fan} q_{test}} = \frac{P_{motor}\eta_{motor}}{A_{test}U_{test}q_{test}} \tag{17}$$

where Δp_{tot} is the total pressure loss in the wind-tunnel circuit that has to be built up by the fan, η_{fan} is the fan efficiency factor, q_{test} is the dynamic pressure in the test section, P_{motor} is the power input, U_{test} is the velocity

rpm	Δp Pa	U m/s	P kW	λ
100	8	3.5	0.02	1.97
200	28	8.1	0.12	0.89
300	61	12.7	0.38	0.72
400	107	17.4	0.83	0.61
500	166	22.2	1.57	0.56
600	237	27.1	2.67	0.53
700	321	32.0	4.19	0.50
800	419	36.9	6.19	0.48
900	528	41.8	8.79	0.47
1000	649	46.6	12.0	0.46

Table 5: Δp over the fan, speed in test section and power factor of the wind-tunnel versus fan speed. λ is calculated using power input with $\eta_{motor} = 0.88$.

in the test section and A_{test} is the cross section area in the test section. In table 5, the power factor is presented for different fan speeds together with the pressure difference over the fan, test section velocity and power input.

Note that there is a strong Reynolds number dependence of λ. This is because the losses in the dominant parts, such as screens and corners, are all strongly dependent on the Reynolds number. Therefore it is important to take into consideration the velocity and the wind tunnel size when comparing power factors of different wind-tunnels. The MTL wind tunnel has a power factor of around 0.39 at a speed of 69 m/s. With the similarities between the MTL and the new wind-tunnel except for the size and the expanding corners it is clear that it is possible to implement expanding corners without substantially increasing the total loss in the wind-tunnel.

3.5 Noise measurements around fan and test section

Low noise levels are important both for the working environment and the measurements since the pressure fluctuations generated by the noise can affect the measurement results. The noise levels presented below are from measurements outside the wind-tunnel circuit since measuring the small pressure fluctuations inside the test section without any influence from the dynamic pressure fluctuations is virtually impossible. It was very encouraging to see that the noise levels were quite low, see figure 26, with the only noise damping being the silencers upstream and downstream the fan.

The peak in the noise outside the fan at 900 rpm is due to bearing problems at certain fan revolutions. This noise however is of quite high frequency and it does not effect the noise level outside the test section.

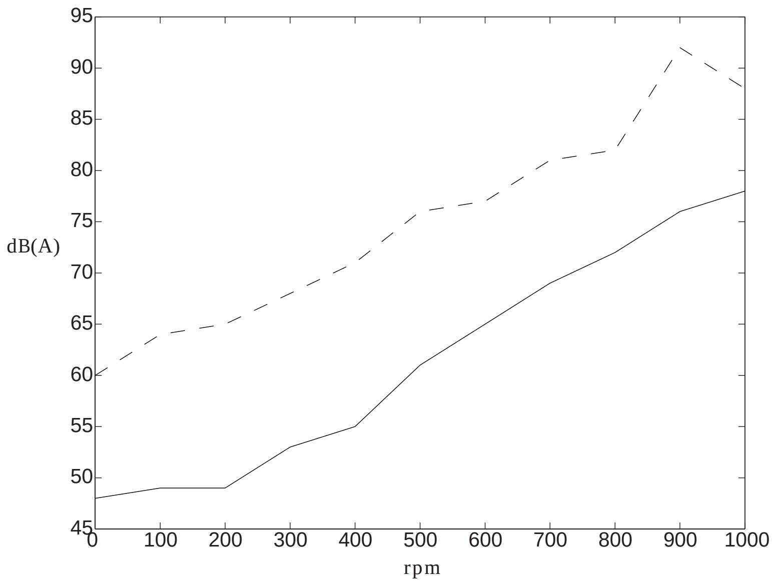

Figure 26: The noise levels just outside the test section (solid line) and outside the fan (dashed line).

3.6 Dynamic pressure measurement downstream corner number 1

To investigate the performance of expanding corners in a wind-tunnel circuit a traversing system, that traverses a Pitot tube across the cascade at the centerline in the cross-stream direction, was inserted into the diffuser downstream the first corner. The experiment was designed to be as similar as possible to the measurements done in [LÖJ] to investigate the possibility to use expanding corners. The expansion ratio is slightly different, $\sqrt[8]{9}$, compared to $\frac{4}{3}$, and the guide-vanes are here the vanes optimized for expanding corners, compared to the MTL-type of vanes in the early measurements. Vane profile differences are illustrated in figure 27.

The interesting quantity to measure is the total pressure loss coefficient, also called the head loss coefficient and since the contribution from the corners to the total losses in the wind-tunnel circuit is about 20 % it is very important that the pressure loss is kept to a minimum. The total pressure loss coefficient of the corner is defined as

$$\frac{\Delta H}{q_0} = \frac{p_{t0} - \overline{p_{t1}}}{q_0} \tag{18}$$

where ΔH is the total head (pressure) loss, q_0 is the dynamic pressure upstream of the corner, p_{t0} is the total pressure upstream of the corner and $\overline{p_{t1}}$ is the mean value of the total pressure downstream of the corner, (figure 28).

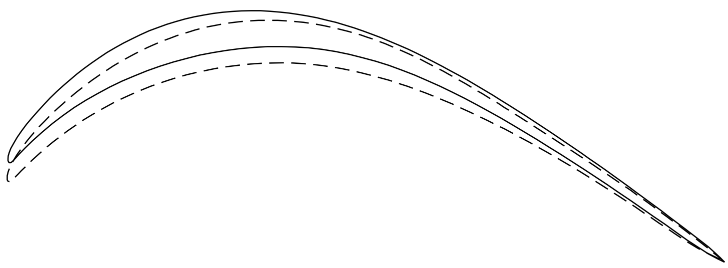

Figure 27: The profiles of the new guide-vane optimized for expanding corners, dashed line, and the scaled-down MTL guide vane, solid line.

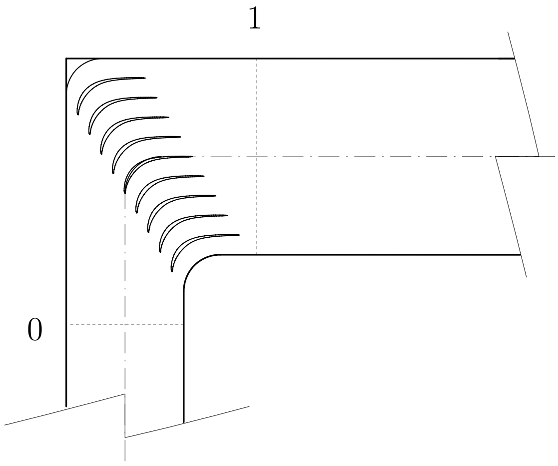

Figure 28: The measuring positions in an expanding corner

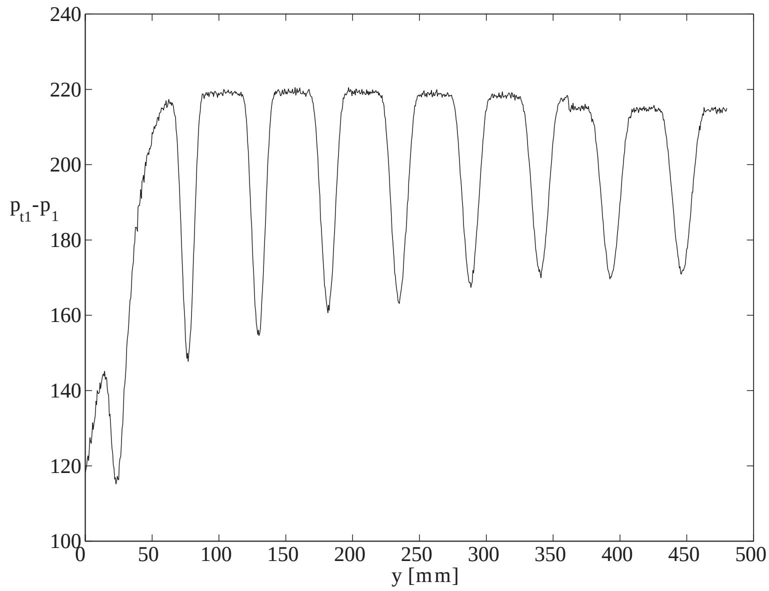

Figure 29: The wake profiles behind the guide-vanes in corner 1.

To be able to measure the total pressure loss, the terms in equation 18 have to be expressed in pressure differences. The expression for the normalized pressure loss reads, (see [LÖJ])

$$\frac{\Delta H}{q_0} = \frac{p_{t0} - p_1 - \frac{1}{nh_1}\int_0^{nh_1} (p_{t1}(y) - p_1)\, dy}{p_{t0} - p_0} \tag{19}$$

where p_{t1} is the total pressure after the corner and p_0 and p_1 are the static pressure before and after the corner respectively. n is the number of vanes over which the integration takes place and h_1 is the outflow distance between the vanes.

The measured pressure profile, seen in figure 29, shows the wake distributions. The uniformity of the flow can also be seen by comparing the regions between the wakes. The inlet flow speed is 19 m/s. The jump in the curve signifies the end of one and the beginning of another set of measurements from two different days. The change of a few pascal is due to different ambient conditions.

Note the thickness of the boundary layers. With $y = 0$ in figure 29 equal to a distance of 43 mm from the wall, the boundary layer thickness is about 125 mm. The fast increase of the pressure around the bend leads to a rapid growth of the boundary layer thickness.

The total pressure loss coefficient, $\frac{\Delta H}{q_0}$, is calculated from the pressure distribution and is equal to 0.046, to be compared with the calculated value of 0.041 in [LÖJ].

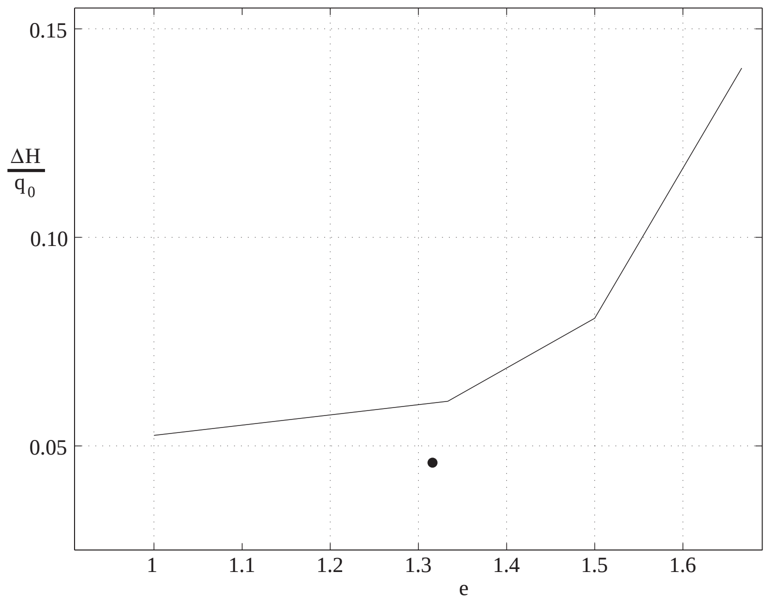

Figure 30: The present measurement result, filled circle, and measurements from [LÖJ], solid line, with the scaled-down MTL guide-vane. The spacing to chord ratio is 0.30 and 0.27 and the Reynolds numbers are 276000 and 200000 respectively.

The Reynolds number based on the chord length and the velocity at position 0 was 276000. This is higher than the highest Reynolds number in the experiments in [LÖJ] which was 225000. On the other hand it was also shown in [LÖJ] that the effect of Reynolds number is very small for Reynolds number above 200000. In figure 30, the present result has been plotted as a filled circle together with measurements of the total pressure loss coefficient versus the expansion ratio using the scaled-down MTL guide-vane.

Note that the spacing to chord ratio is 0.30 for the present measurement compared to 0.27 for the measurements from [LÖJ]. The effect of the spacing to chord ratio is plotted in figure 31. Here the expansion ratio is 1.33 for the measurements from [LÖJ]. This value is very close to the expansion ratio in the new wind-tunnel, $e = 1.316$.

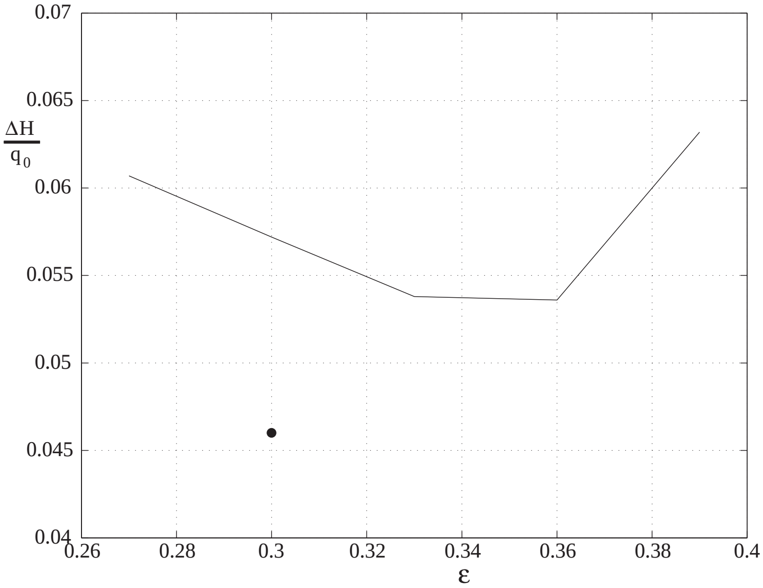

Figure 31: The effect of spacing to chord ratio, ϵ, present measurement, filled circle, and measurements from [LÖJ], solid line.

4 Acknowledgments

I would like to thank Ulf Landén who has been working on assembling the wind-tunnel parts since the project started. I also like to thank Marcus Gällstedt and Jens Österlund for help during the construction process and my supervisor, professor Arne Johansson, for his support. The author also wish to thank Dr Magnus Hallbäck for efforts in the early stages of the planning. Funding from the Göran Gustafsson Foundation and TFR is greatfully acknowledged.

References

[Collar, 1936] Collar, A. R. (1936). Some experiments with cascades of aerofoils. A.R.C. Technical Report 1768, Aeronautical research committee.

[Friedman and Westphal, 1952] Friedman, D. and Westphal, W. R. (1952). Experimental investigation of a 90° cascade diffusing bend with an area ratio of 1.45:1 and with several inlet boundary layers. TN 2668, NACA.

[Groth and Johansson, 1988] Groth, J. and Johansson, A. V. (1988). Turbulence reduction by screens. *J. Fluid Mech*, 197:139–155.

[Johansson, 1992] Johansson, A. V. (1992). A low speed wind-tunnel with extreme flow quality-design and tests. *Proc. the 18:th ICAS Congress*, pages 1603–1611.

[Kröber, 1932] Kröber, G. (1932). Schaufelgitter zur Umlenkung von Flussigkeits-Strömung. *Ingenieur-Archiv*, 3:516.

[Laws and Livesey, 1978] Laws, E. and Livesey, J. (1978). Flow through screens. *Ann rev Fluid Mech.*, 10:247–266.

[Lindgren et al., 1998] Lindgren, B., Österlund, J., and Johansson, A. V. (1998). Design of guide vanes for minimizing the pressure loss in sharp bends. *Experiments in Fluids*, 24:265–272.

[Taylor and Batchelor, 1949] Taylor, G. and Batchelor, G. K. (1949). The effect of wire gauze on small disturbances in a uniform stream. *Quart. J. Mech. and App. Math.*, 2:part 1,1.

[Wolf, 1957] Wolf, H. (1957). Messungen im Nachlauf eines Gleichdruckgitters für 90°-umlenkung. *Maschinenbautechnik*, 6(10):539.

A Drawings

A.1 Test section

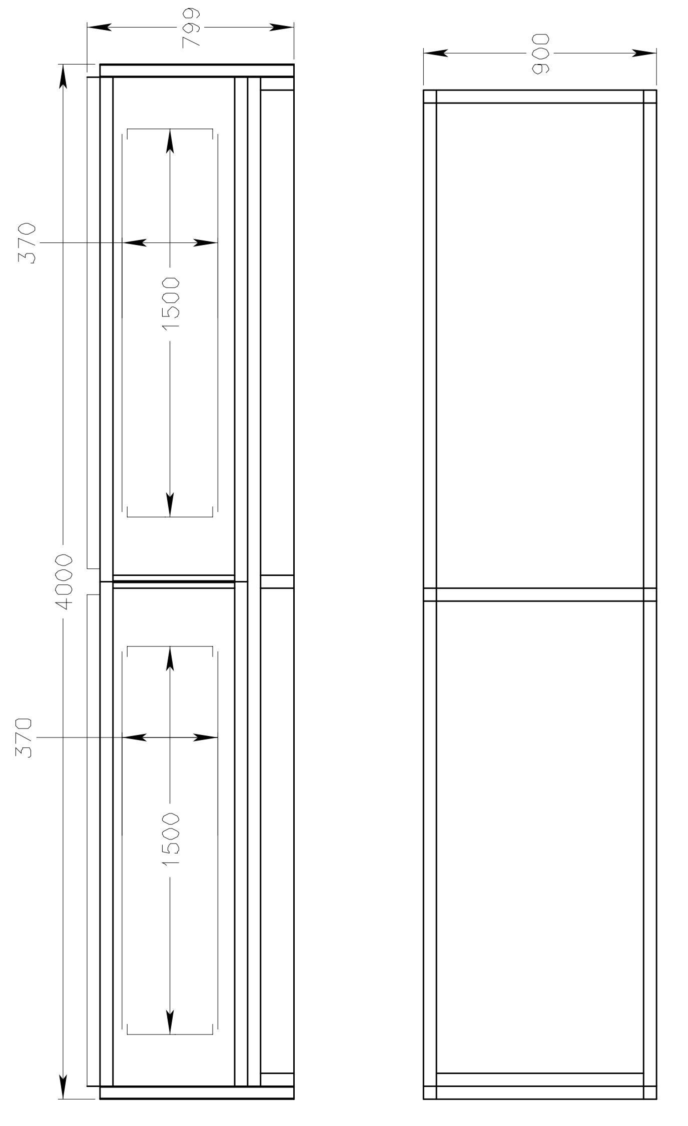

Figure 32: test section

A.2 Diffusers

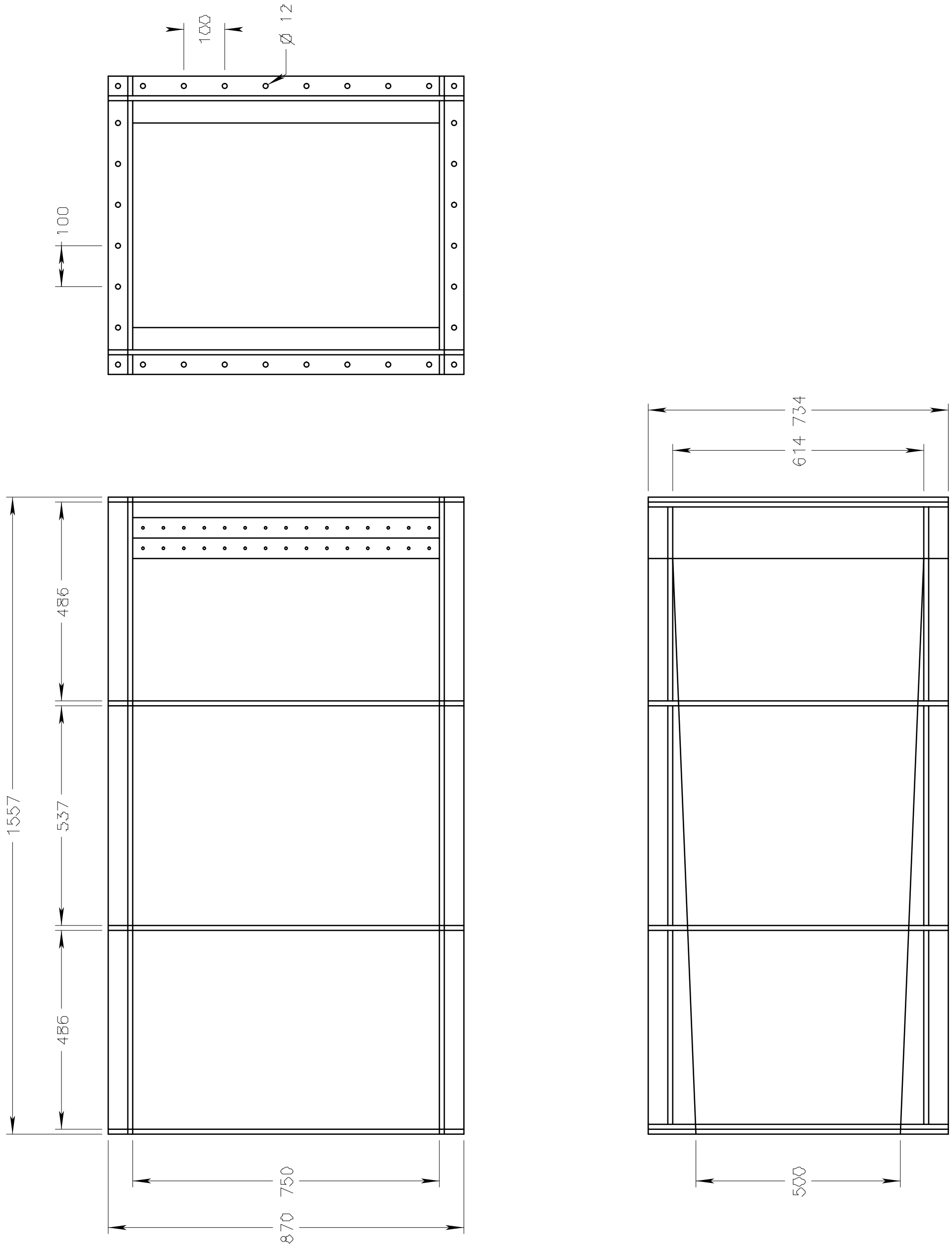

Figure 33: diffuser 1

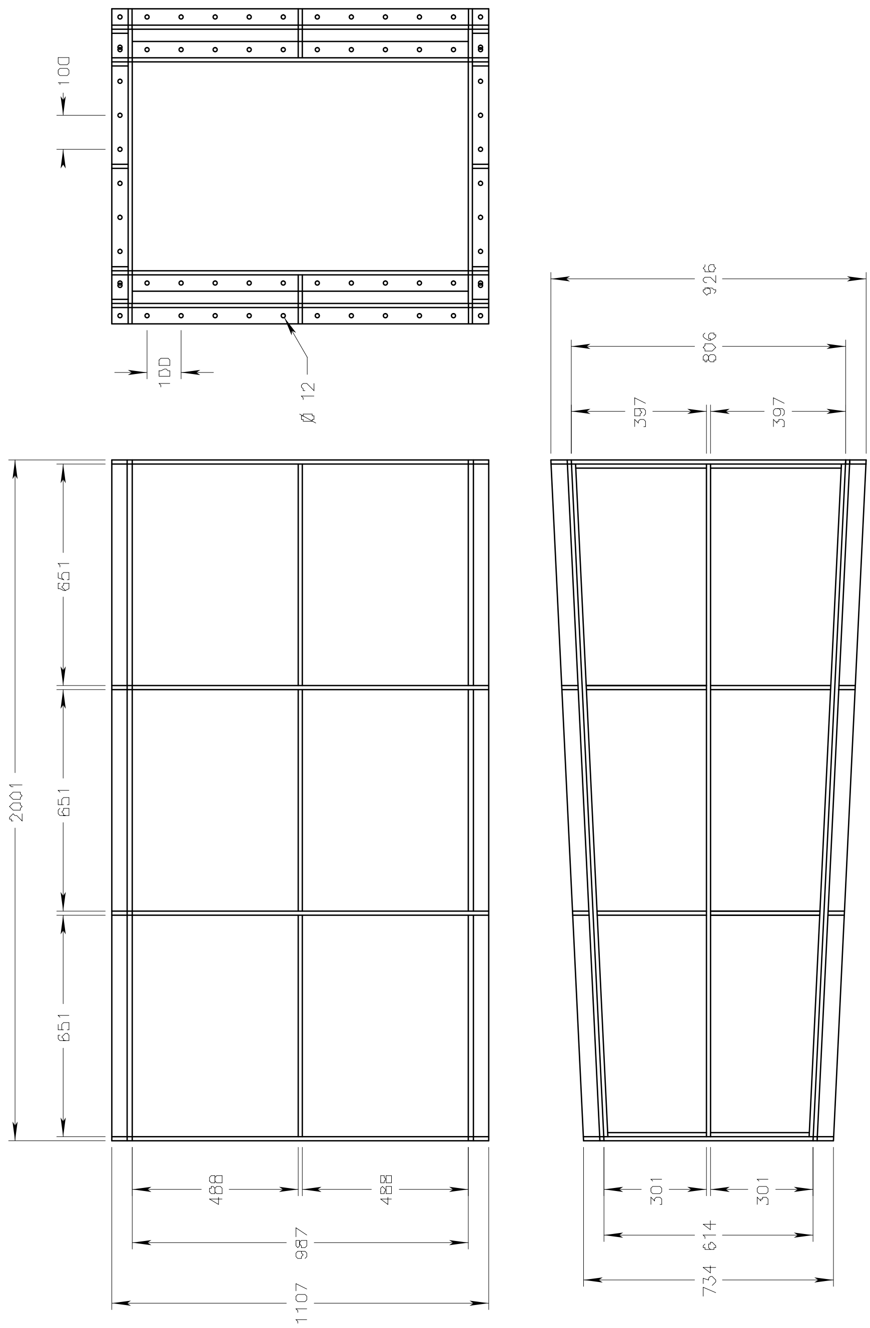

Figure 34: diffuser 2

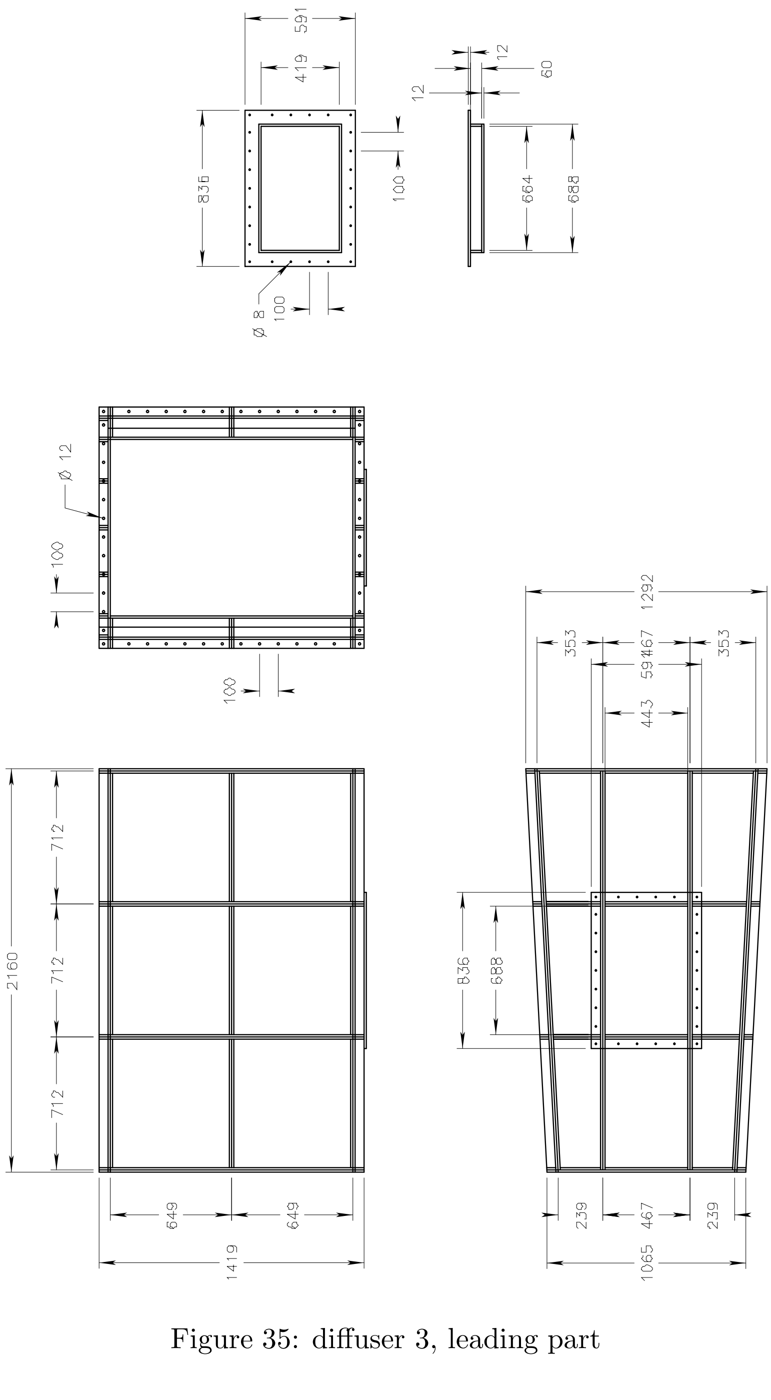

Figure 35: diffuser 3, leading part

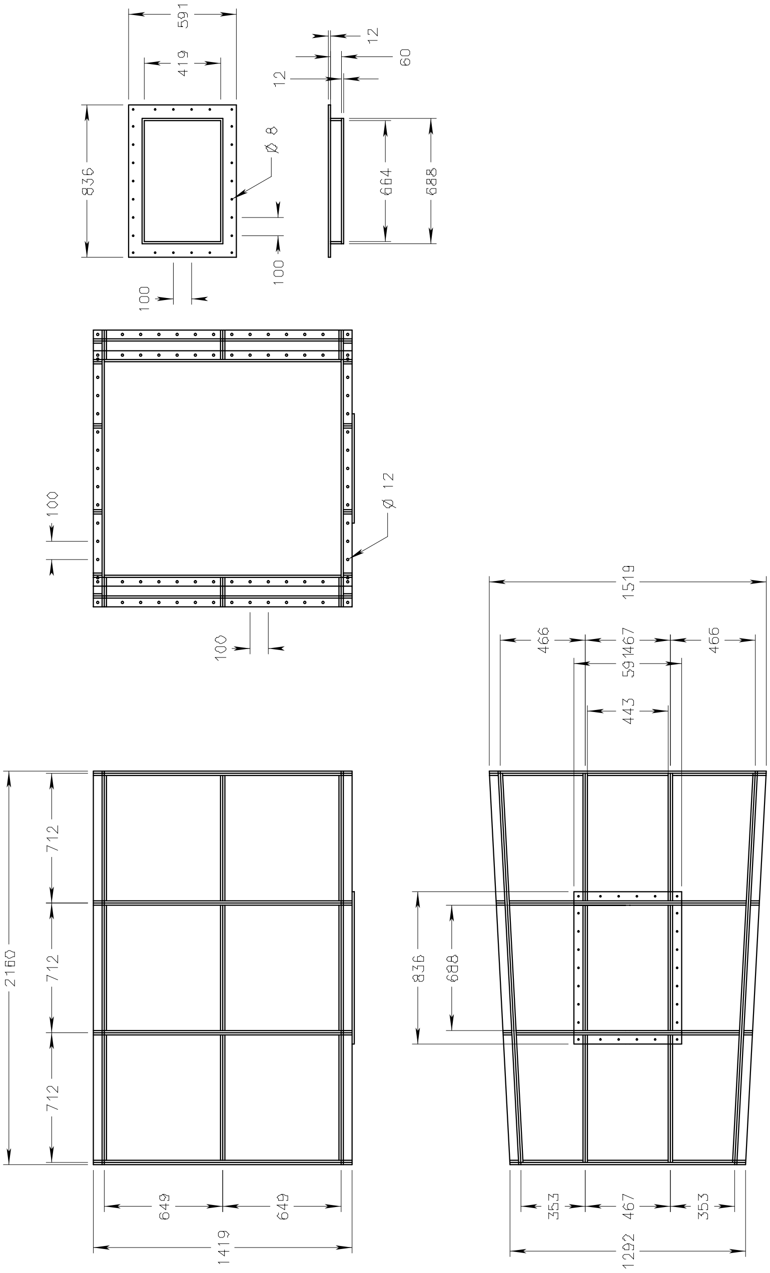

Figure 36: diffuser 3, trailing part

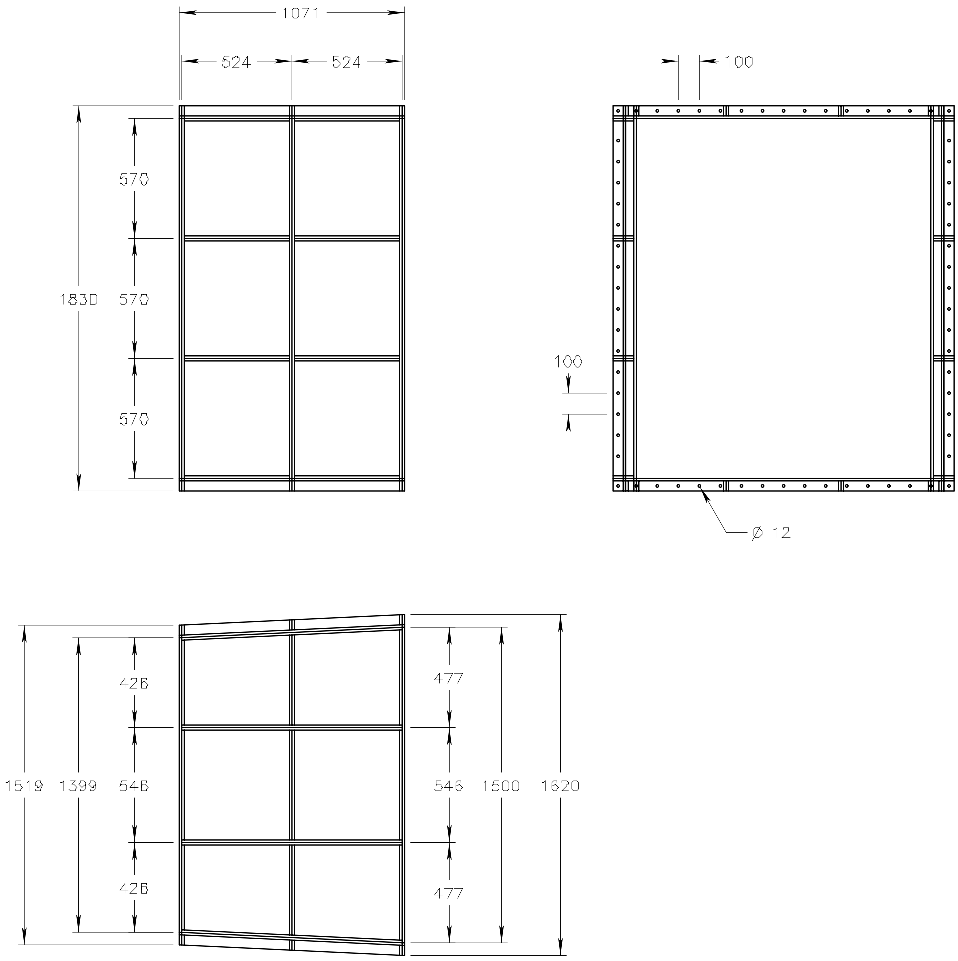

Figure 37: diffuser 4

A.3 Corners

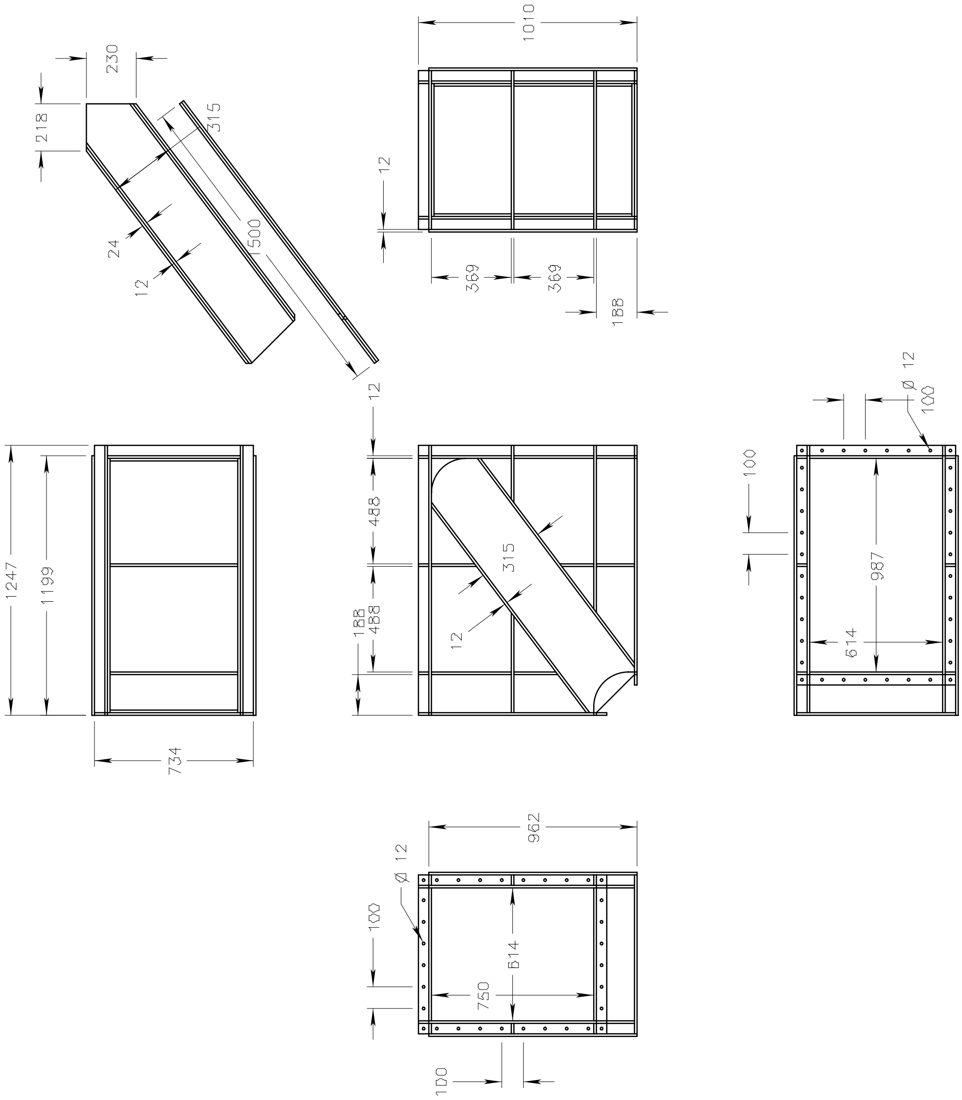

Figure 38: corner 1

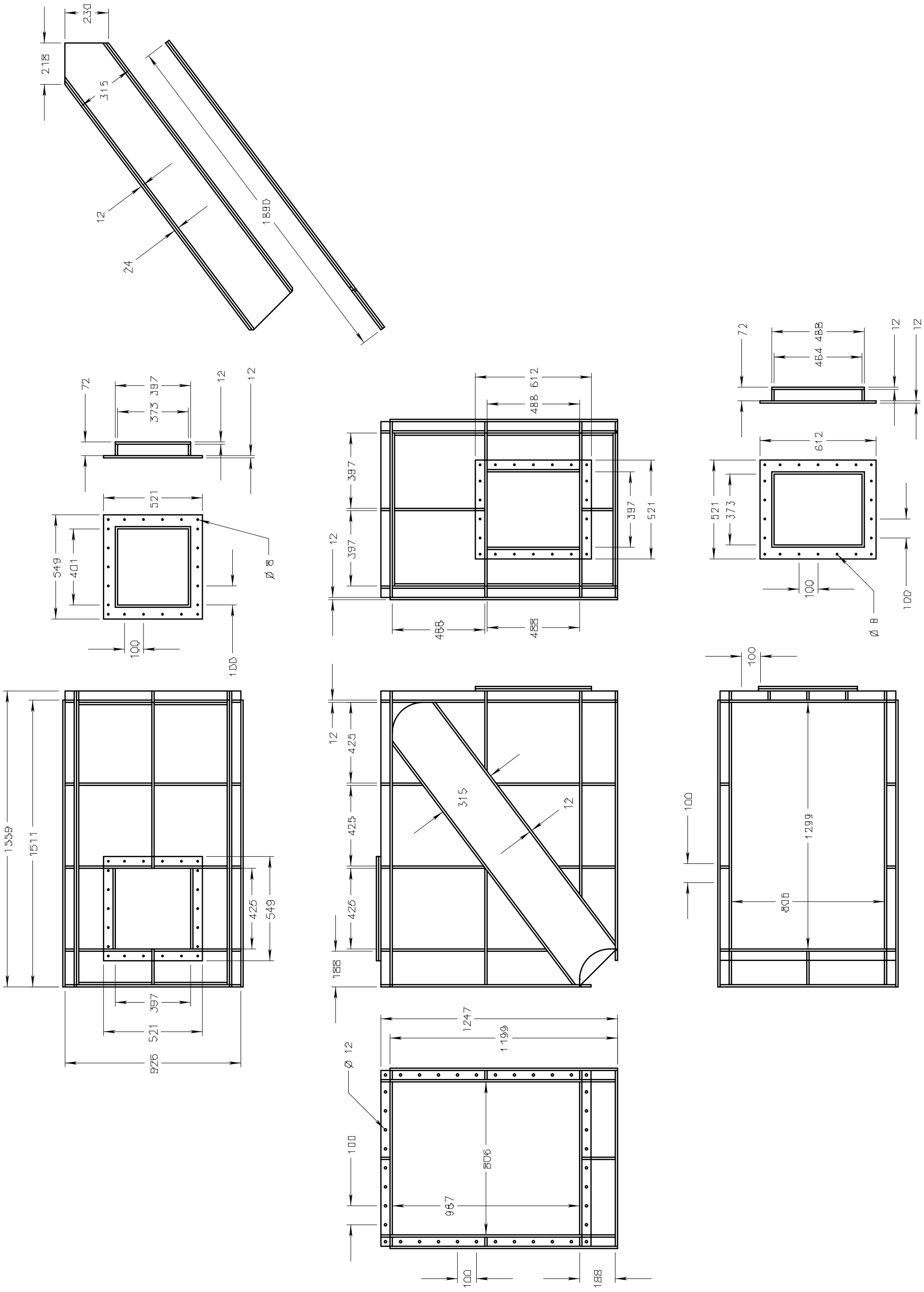

Figure 39: corner 2

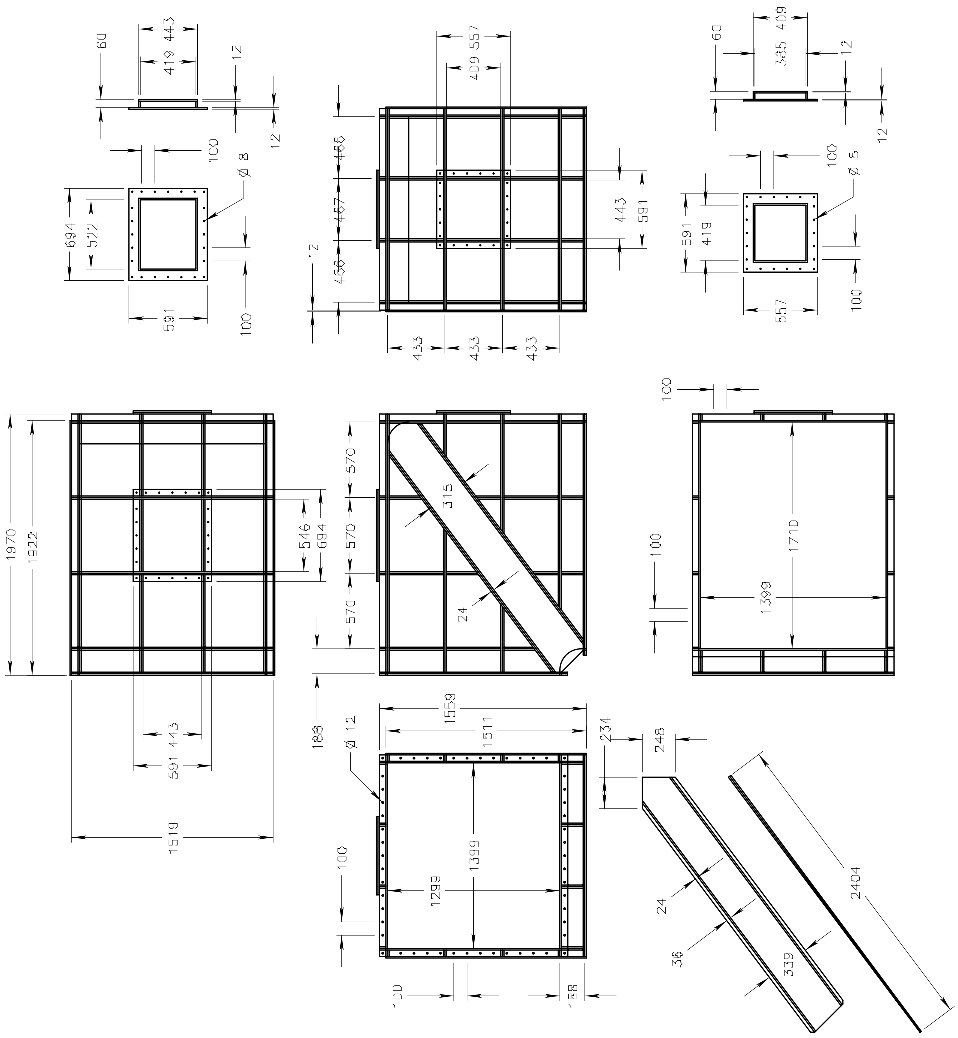

Figure 40: corner 3

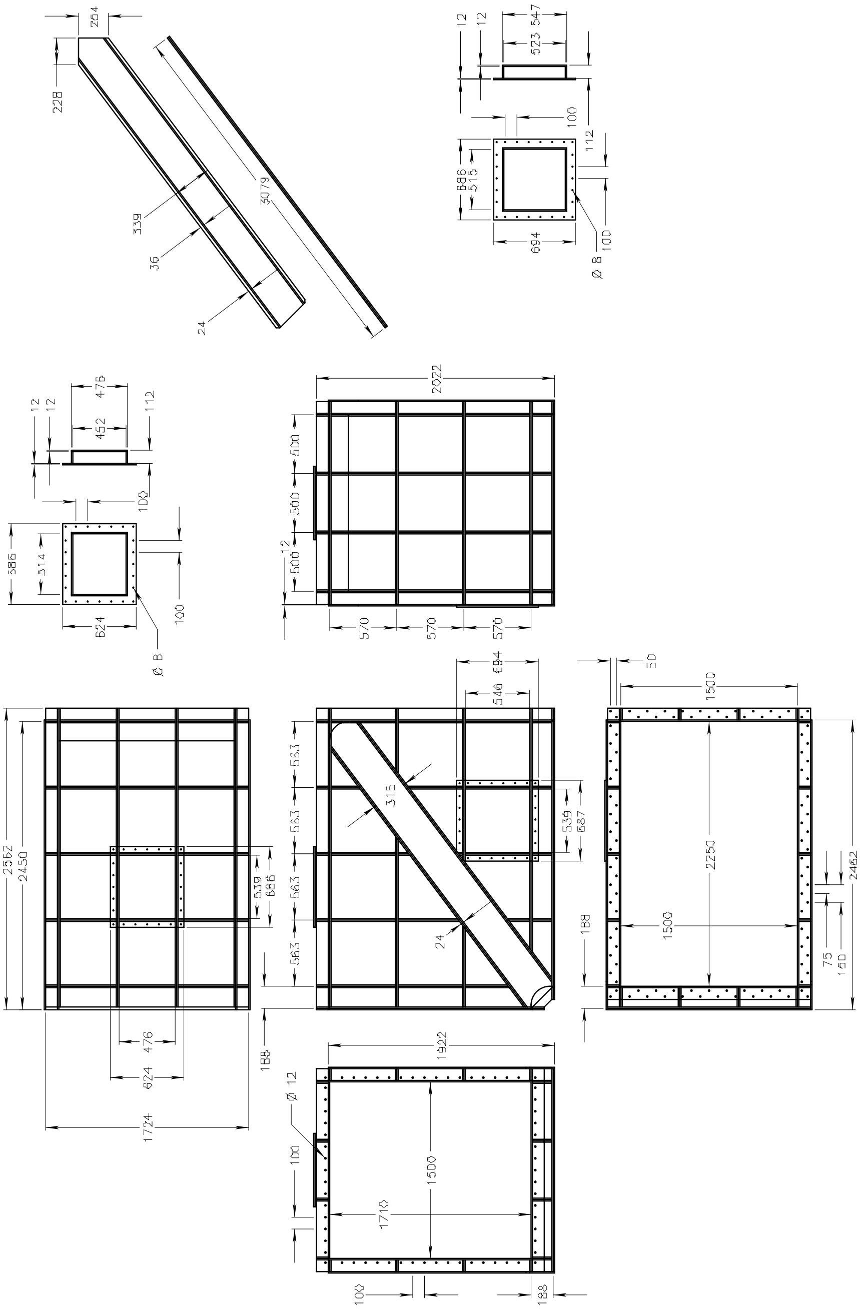

Figure 41: corner 4

A.4 Stagnation chamber and contraction

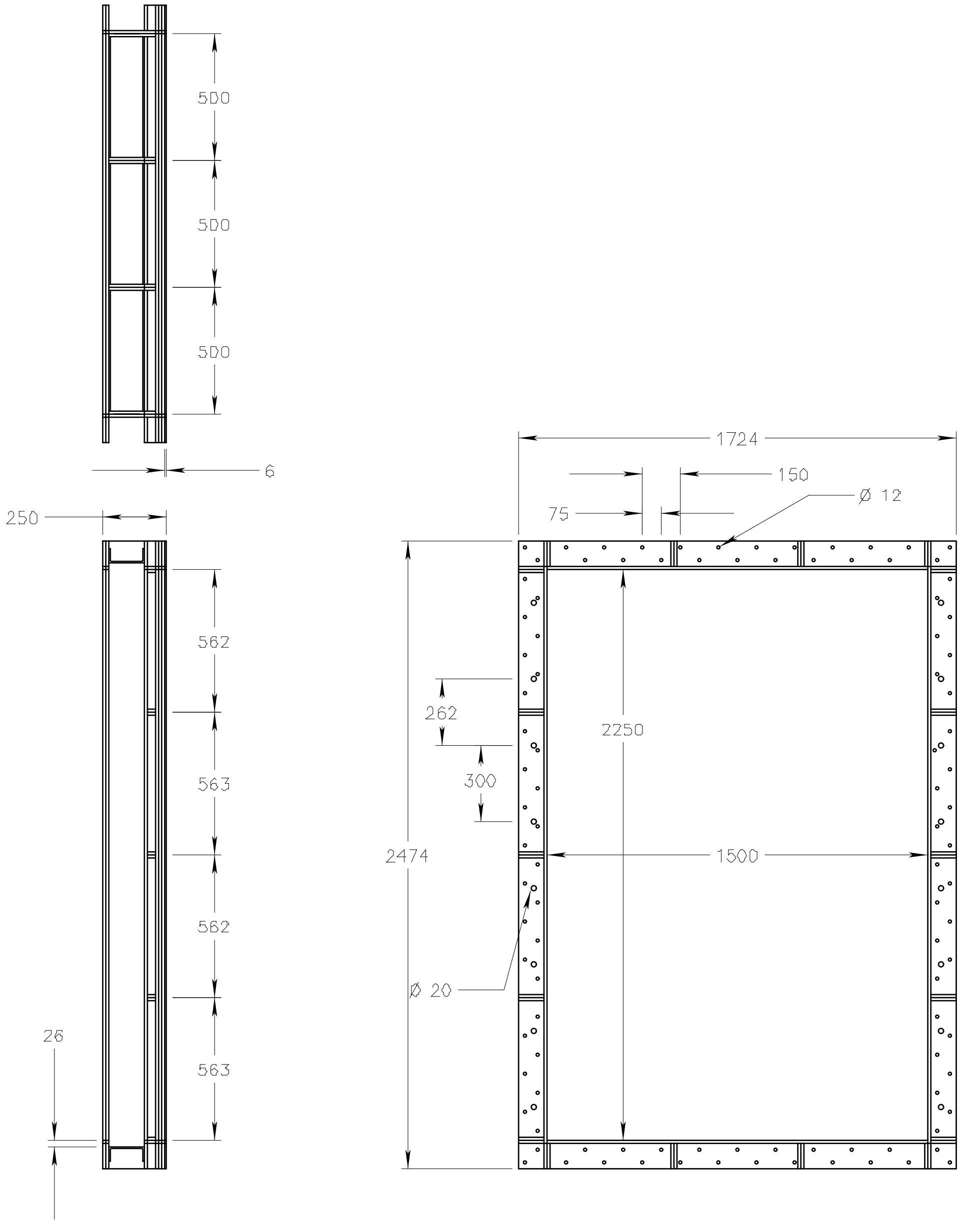

Figure 42: honeycomb frame

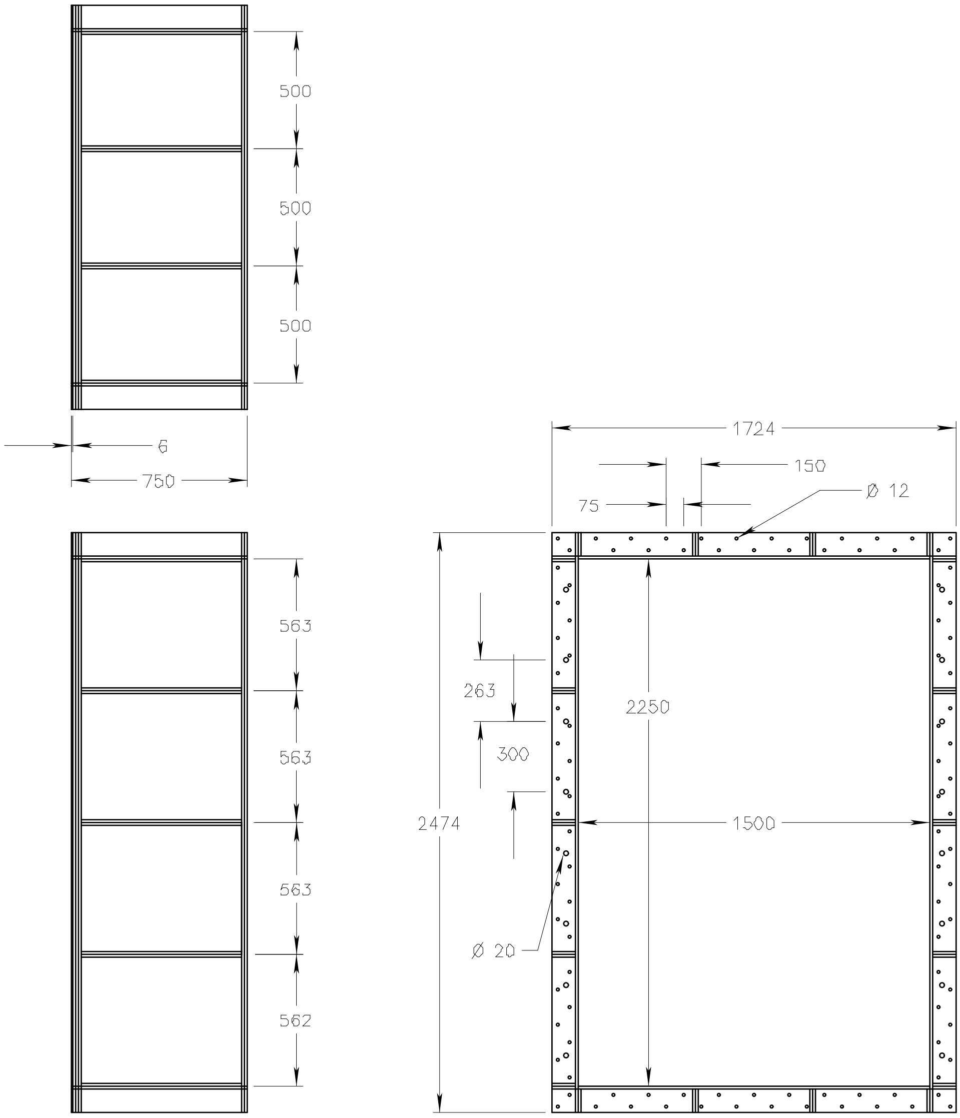

Figure 43: stagnation chamber

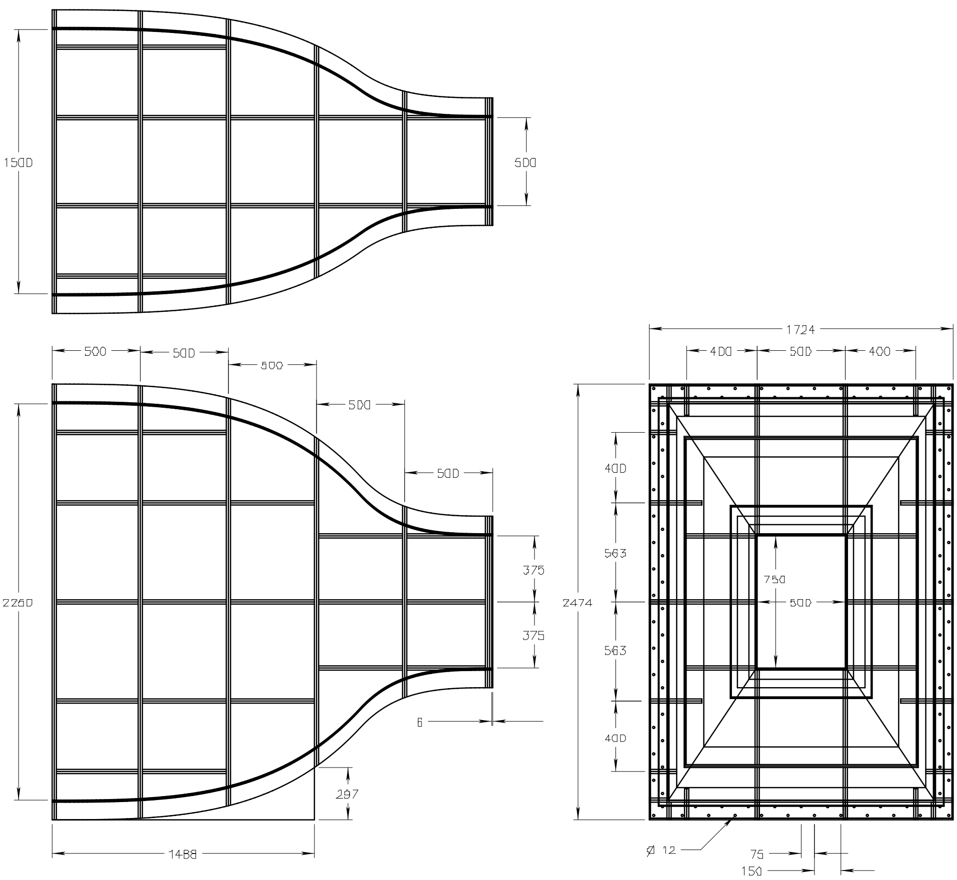

Figure 44: contraction

A.5 Driving unit

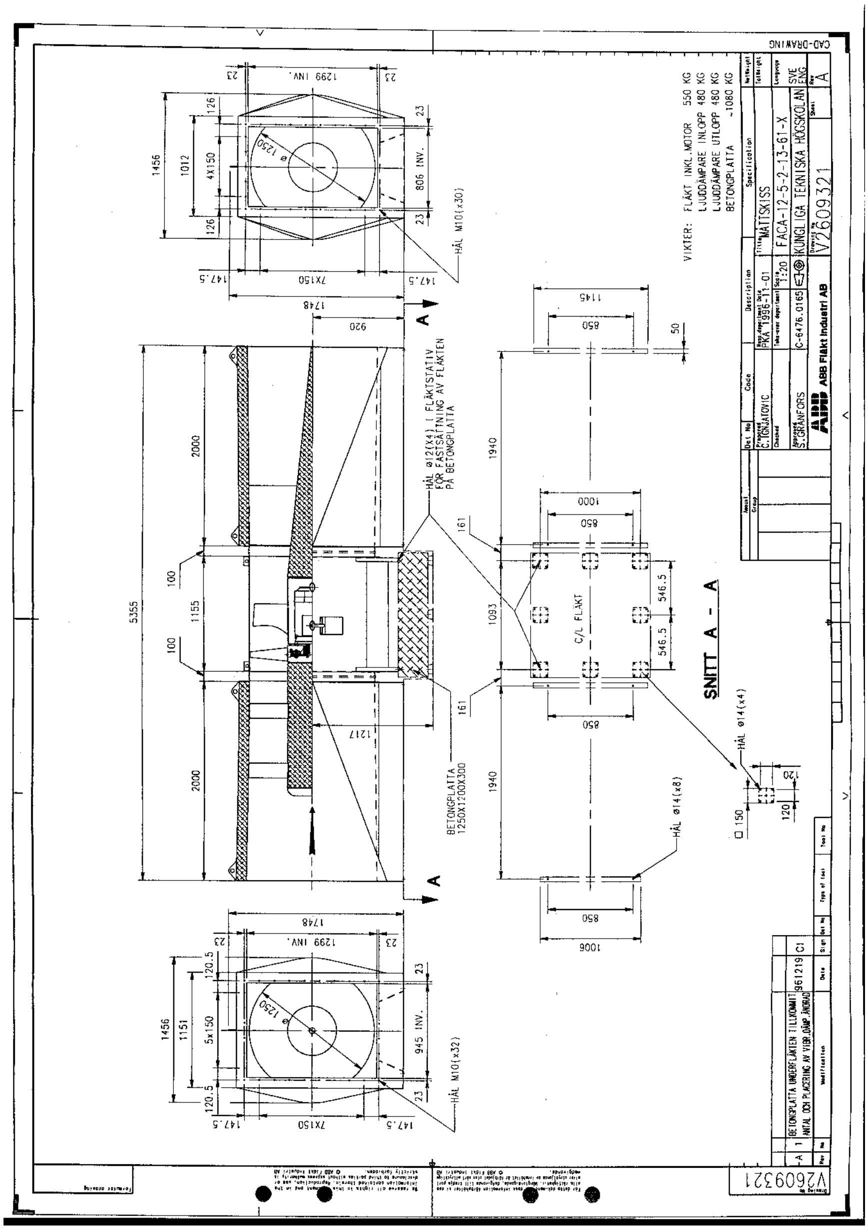

Figure 45: driving unit including fan motor and silencers

A.6 Cooling system

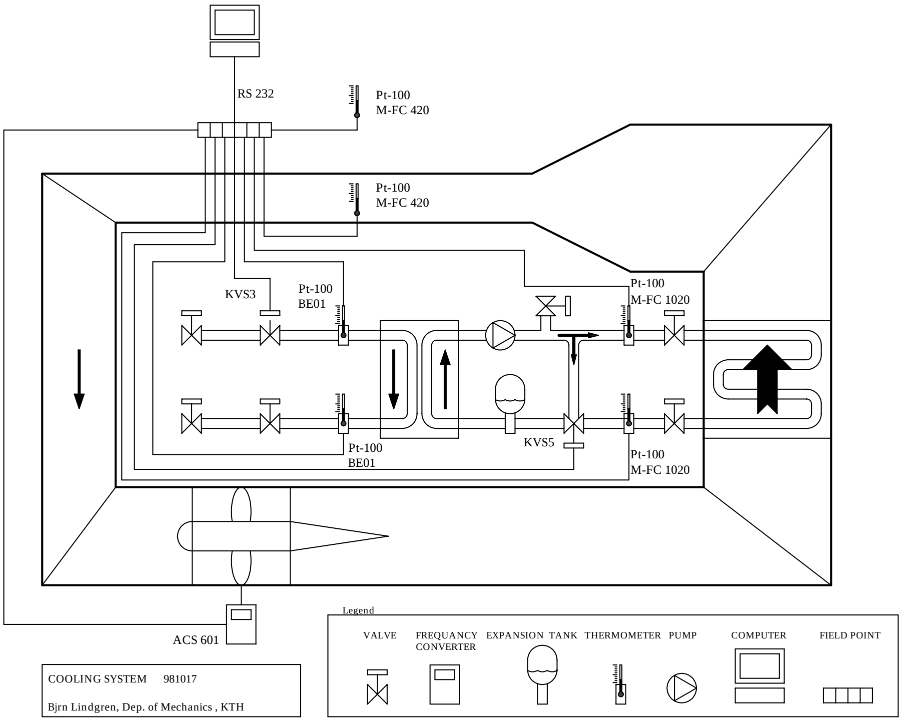

Figure 46: cooling control loop

A.7 Electrical scheme

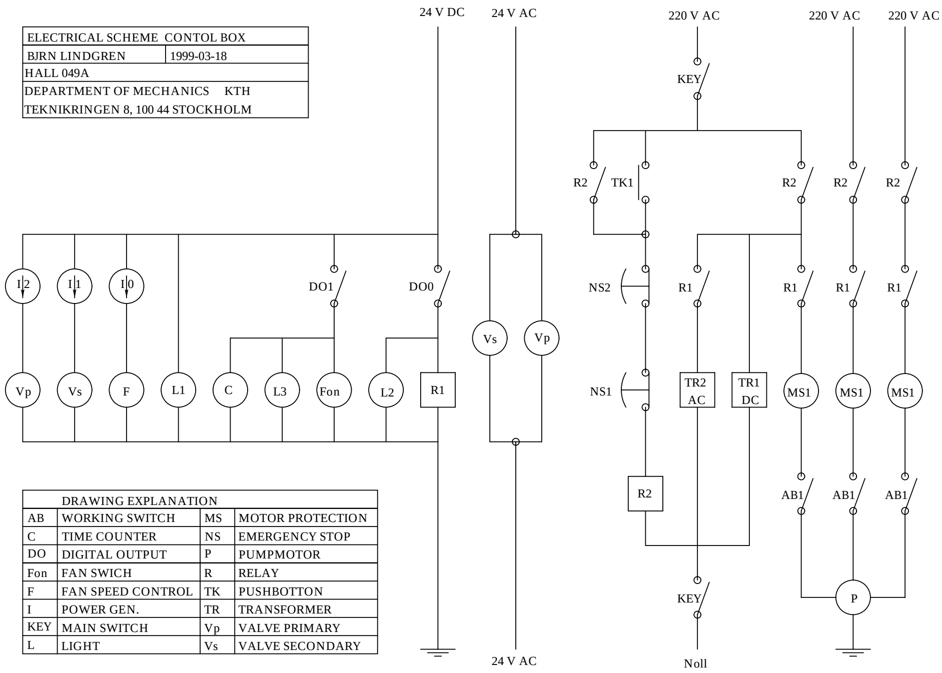

Figure 47: electrical scheme for the control unit